The Convergence of Heat, Groundwater & Fracture Permeability:

Innovative Play Fairway Modelling Applied to the Tularosa Basin

DOE Contract #DE-EE0006730

◼ PHASE 2 PROJECT REPORT ◼

May 31, 2017

Submitted By:

Ruby Mountain Inc.

Salt Lake City ◼ El Paso ◼ Seattle ◼ Newport Beach

and

EGI Energy & Geoscience Institute
AT THE UNIVERSITY OF UTAH

The Convergence of Heat, Groundwater & Fracture Permeability:

Innovative Play Fairway Modelling Applied to the Tularosa Basin

◼ PHASE 2 PROJECT REPORT ◼

This report is submitted to the U.S. Department of Energy (DOE) in fulfillment of requirements of Contract #DE-EE0006730 which was awarded to develop a methodology for, and conduct, a Geothermal Play Fairway Analysis in the Tularosa Basin located in South-Central New Mexico and Far West Texas. Ruby Mountain Inc. (RMI) is the prime contractor to DOE under the grant award. The Energy and Geoscience Institute (EGI) at the University of Utah is the prime subcontractor to RMI.

This report summarizes the activities and key findings of the project team occurring during Phase 2 (primarily from August 2016 – May 2017) of the Tularosa Basin Geothermal Play Fairway Analysis Project. Questions regarding the contents of this document should be directed to: RMI Senior Project Manager Carlon R. Bennett at carlonbennett@gmail.com

Submitted By:

Ruby Mountain Inc.

Carlon R. Bennett, Project Manager
2373 East 1300 South, Salt Lake City, UT 84108
801-538-5003 ● rubymountaininc.com

and the

EGI Energy & Geoscience Institute
AT THE UNIVERSITY OF UTAH

Gregory D. Nash, Ph.D. Principal Investigator
423 Wakara Way #300, Salt Lake City, UT 84108
801-581-5126 ● egi.utah.edu

TABLE OF CONTENTS

ACKNOWLEDGEMENTS

PROJECT TEAM

Ruby Mountain Inc.
- Carlon R. Bennett, PFA Project Manager
- Jon Lear, RMI Principal
- Jesus Daniel Aguilar, Administrative Assistant to the Project Manager

Energy & Geoscience Institute at the University of Utah
- Gregory Nash, Ph.D., Project Principal Investigator
- Phil Wannamaker, Ph.D., Research Professor
- Stuart Simmons, Ph.D. Research Professor
- Rasoul B. Sorkhabi , Ph.D., Research Professor
- Virginia Maris, Ph.D., Post Doc.
- Adam Brandt, Student Research Assistant
- Brian Pfaff, Student Research Assistant

U.S. Navy Geothermal Program Office
- Michael Lazaro, Navy Geothermal Division Director
- Kelly Blake, P.G., Geologist
- Andrew Sabin, Ph.D., P.G., Geologist
- Saundra Anderson, GPO Business Manager

Utah Geologic Survey
- Mark Gwynn, P.G., Geologist
- Christian Hardwick, P.G., Geophysicist
- Jodi Patterson, UGS Financial Manager

Barker Engineering
- Benjamin Barker, P.E., Special Project Consultant

Quantech Geoscience, Ltd.
- Jeff Nichols, Debbie Ramlal and Jeff Violette

The Convergence of Heat, Groundwater & Fracture Permeability:

Innovative Play Fairway Modelling Applied to the Tularosa Basin

Greg Nash[1], Carlon Bennett[2], Stuart Simmons[1], Kelly Blake[3], Christian Hardwick[4], Mark Gwynn[4], Rasoul Sorkhabi[1], Virginia Maris[1], Phil Wannamaker[1], Andrew Sabin[3], Adam Brandt[1], Brian Pfaff[1]

[1]Energy & Geoscience Institute at the University of Utah, [2]Ruby Mountain, Inc., [3]Navy Geothermal Program Office, [4]Utah Geological Survey

1.0 OVERVIEW

1.1 Introduction
This Phase 2 Report for the Tularosa Basin Play Fairway Analysis (PFA) Project is submitted to the U.S. Department of Energy (DOE) in fulfillment of requirements of Contract #DE-EE0006730 which was awarded to develop a methodology for, and conduct, a Geothermal Play Fairway Analysis in the Tularosa Basin located in South-Central New Mexico and Far West Texas. Ruby Mountain Inc. (RMI) is the prime contractor to DOE under the grant award. The Energy and Geoscience Institute (EGI) at the University of Utah is the prime subcontractor to RMI. This report summarizes primary activities and key findings of the project team occurring during second phase work from July 2016 – May 2017.

1.2 Phase 2 Planning and Work
Phase two work successfully fulfilled our three main objectives: (1) fill in data needed for play fairway analysis (PFA) which was missing or sparse in identified Phase 1 plays; (2) collect local datasets in high priority areas; and, (3) become more familiar with the geology of all identified plays. As importantly, our second phase efforts continue to demonstrate that the play fairway methodology developed by our team, while complex, has the unique ability to be easily understood by decision makers of all varieties – having been well received by both military leadership and energy staff at several installations.

The project team's Phase 2 work plan consisted primarily of the following:
1. Field geology
   a. Geological reconnaissance at low priority plays
   b. Mapping, with an emphasis on structure, at high priority plays
2. Gravity data surveys and infill at high priority plays
3. Shallow temperature (2m) surveys at high priority plays
4. Existing well water sampling for chemical analyses and geothermometry
5. Temperature logging in existing wells
6. A magnetotelluric survey at McGregor Range to support future drilling
7. New PFA model development

It was originally anticipated that water chemistry and/or temperature gradient data would be collected from each play regardless of priority, with the exception of McGregor Range, for which a relatively rich

data set already exists. However, in reality, wells were not accessible in all plays during our Phase 2 data collection period. Figure 1 shows plays for which new data were collected.

1.3 Study Area

The Tularosa Basin is a graben located in the southern Rio Grande Rift (Fig. 2). The study area covers approximately 7,700 miles^2, much of which is underexplored. Several factors went into the selection of the Tularosa Basin. It was primarily chosen because it is a challenging, yet ideal test bed to evaluate effectiveness of PFA.

The basin is home to several military installations including White Sands Missile Range (WSMR) and Fort Bliss, which are the first and second largest U.S. Army bases in the United States, together covering more than 10,000 km^2 of southcentral New Mexico and Far West Texas. Both installations have been cooperative throughout our geothermal exploration efforts and have expressed an interest in developing any geothermal resource which may be proven viable.

Additionally, the Aerospace Data Facility Southwest (ADF-SW) located at the Johnson Space Center's White Sands Test Facility on the western side of the Organ Mountains requested to join Phase 2 of the Tularosa Basin PFA effort in summer of 2016 and provided funding for the RMI project team to begin exploration on the western side of the Organ Mountains. The DOE agreed to the addition and ADF-SW provided funding to supplement the existing DOE project grant. The RMI team provided a 20 percent cost share to the ADF-SW funding and was able to bring some economic efficiency to the effort by reducing mobilization/de-mobilization costs for teams already working in the field on the eastern side of the Organ Mountain Range. Geothermal development throughout the basin can help the military achieve its Net Zero Energy goals and installation resiliency objectives.
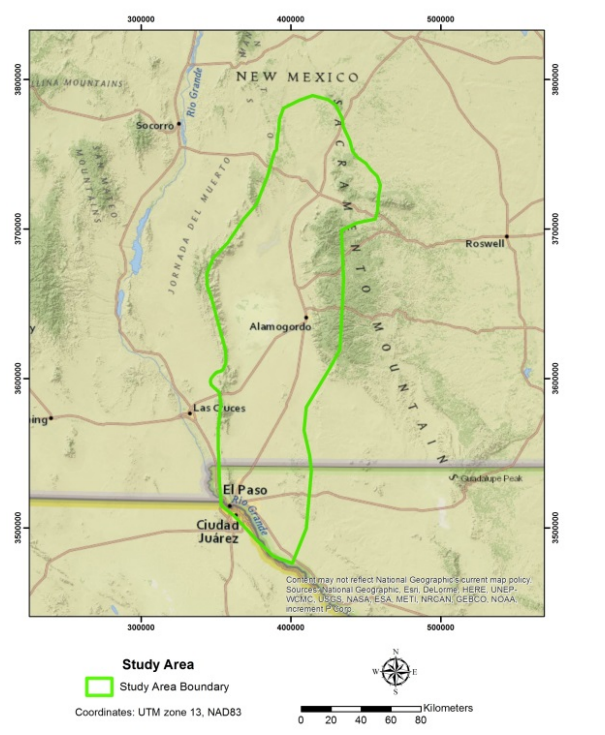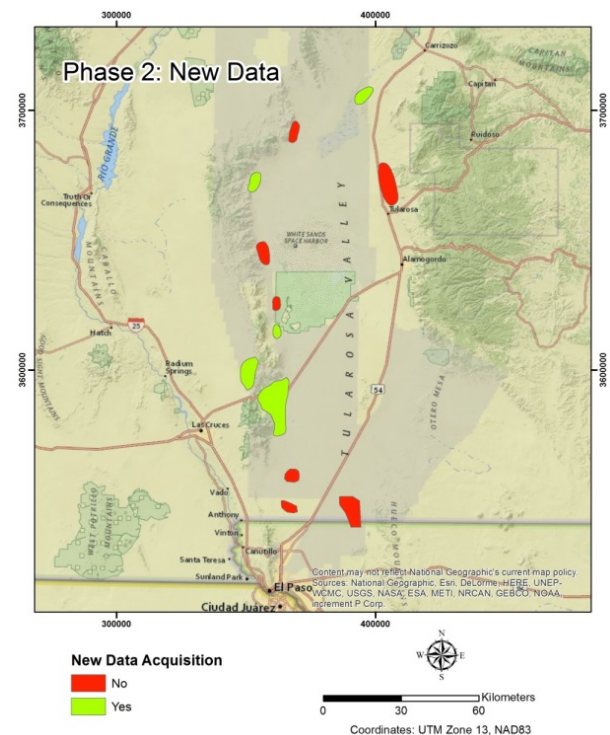

Figure 1. New data collection in plays.

Figure 2. Study area.

2.0 PHASE 2 ACCOMPLISHMENTS

2.0.1 Geology

The study area encompassing the Organ, San Agustin, San Andres, and Sacramento Mountains underwent basement uplift during the early Cenozoic Laramide orogeny. The San Andres, San Agustin, and Sacramento mountains are composed largely of Paleozoic carbonates and quartzite, with local outcrops of Proterozoic granite, and Mesozoic sandstones and conglomerates. The Organ Mountains are predominated by Oligocene granitic rock. Tertiary volcanic rocks are also present locally throughout much of the area. A generalized stratigraphic column can be seen in Appendix A.

Based on mapping and observations reported by Seager (1981), we suggest that the area near the WSMR main cantonment was formed by oroclinal bending during the Laramide. This area was later associated with the emplacement of the 33-Ma Organ Batholith. Basin-and-Range type extension was then superimposed on the Laramide uplift, creating a large number of normal faults bounding grabens and half-grabens. Oroclinal bending structures have often found to be areas of structural complexity and focused strain (e.g., Marshak, 2004). In many areas, extensional basins associated with oroclinal bending are characterized by high heat flow; e.g., Rhine Graben (Pribnow and Clauser, 2000).

Remote sensing and surface mapping have revealed the presence of Quaternary fault systems in the study area. Seager (1981), for instance, documents varying heights of scarps cut by several generations of Quaternary fans. Certain geological features make the study area in this project favorable for geothermal systems: (1) the shallow-level Precambrian and Tertiary igneous rock complex help conduct basement heat flow; (2) structural complexity and focused strain indicates the presence of a networks of structures of medium to small size; (3) active (Quaternary) tectonics suggests structures that are still fluid conductive in some areas (not healed by long-term geological processes); and (4) rift tectonics and magmatism tend to elevate geothermal gradient.

To further advance our knowledge of the area geology, all low priority plays were visited and geologic features of interested noted. One of the priorities in this reconnaissance was to try to identify surficial geothermal features, such as fossil sinters and hydrothermal alteration. Hydrothermal alteration was observed in a small area, along what is believed to be a Quaternary fault, in San Agustin Mountains a few miles north of the WSMR main cantonment. Areas of alteration were also observed in the San Andreas Range; however, these are likely related to the Proterozoic granite that is part of the Laramide thrust package. In the south-eastern corner of the ADFSW play, pervasive silicification of Paleozoic carbonates was noted and several limestone beds in the adjacent range were silicified at different stratigraphic levels suggesting sporadic pulses of hydrothermal actively. This was found to be a structurally complex area containing several copper deposits that attest to past structurally-controlled hydrothermal activity.

Within the high priority areas in WSMR, the Main Cantonment area and adjoining HTA area to the north, several previously unmapped faults were identified. Additionally, numerous mafic, rhyolitic, and granitic pegmatite dikes occur in Proterozoic granite in these areas, which appear to be structurally controlled. The mafic dikes are sometimes accompanied by copper mineralization. New structural details discovered during this work will be discussed further in the gravity data section later in the report.

2.0.2 Water Chemistry and Geothermometry
Geochemical analyses were obtained on shallow groundwater samples (~120 m depth) within the study area. The samples were collected by the Utah Geological Survey in the period November 20 to December 15, 2016, from flowing wells either from storage tanks or from a tap the wellhead (Fig. 3). They were delivered to EGI and then sent out to three separate labs for chemical and isotopic analyses.

2.0.2.1 Methods & Results
Well waters were collected into three different types of containers depending on the methods of analysis. Untreated waters were collected in glass bottles fitted with a rubber tube and hose clamp. These bottles are designed to be over-filled with water and then clamped to prevent loss of aqueous carbon dioxide. The waters were analyzed for bicarbonate (HCO_3) and pH via automated alkalinity titration at the Utah Department of Health lab in Salt Lake City.

Treated samples were collected in acid washed Nalgene bottles (250 ml) for analyses of major anions and cations (Li, Na, K, Ca, Mg, SiO_2, Cl, F, SO_4). These waters were treated in the field first by filtering (0.45 μm) and then by acidification (2.5 mls 10% HNO_3) to preserve the solutes. These samples were analyzed in the Department of Earth Sciences, University of Minnesota. The cations (Li, Na, K, Ca, Mg, SiO_2) were analyzed by ICP-OES and the anions (Cl, F, SO_4) were analyzed by ion chromatography.
Untreated water samples were also collected in 30 ml glass bottles with a screw cap to determine the oxygen (18O/16O) and hydrogen (D/H) isotope ratios. The isotope ratios were measured via mass spectrometers in the SIRFER lab at the University of Utah.

2.0.2.2 Interpretation
The stable isotope compositions of the waters plot as a coherent continuous linear trend that coincides with local ground water (Fig. 4), with the exception of SC-2 (Stallion Range Control Center). The variation in isotopic compositions for all samples reflect fractionation effects due to latitude and/or elevation which is commonly seen in cold shallow groundwaters. Thus the outlying position of SC-2 simply suggests that it comes from percolation of rainwater and/or snowmelt, which entered the ground water system at a higher elevation relative to the rest of the samples. None of the waters show a positive-shift to the right of meteoric water line, as is typical of deeply circulated thermal waters that have been subject to re-equilibration due to high temperature (100-300°C) water-rock interaction.

The waters are near neutral pH (6-7), and the Cl-HCO_3-SO_4 ternary plot (Fig. 5) shows that most of the waters are rich in bicarbonate and/or sulfate. The most sulfate-rich waters are ORC, SC-2 and 100-C-365, whereas the only chloride-rich water is WSRM up-range Herbie well.
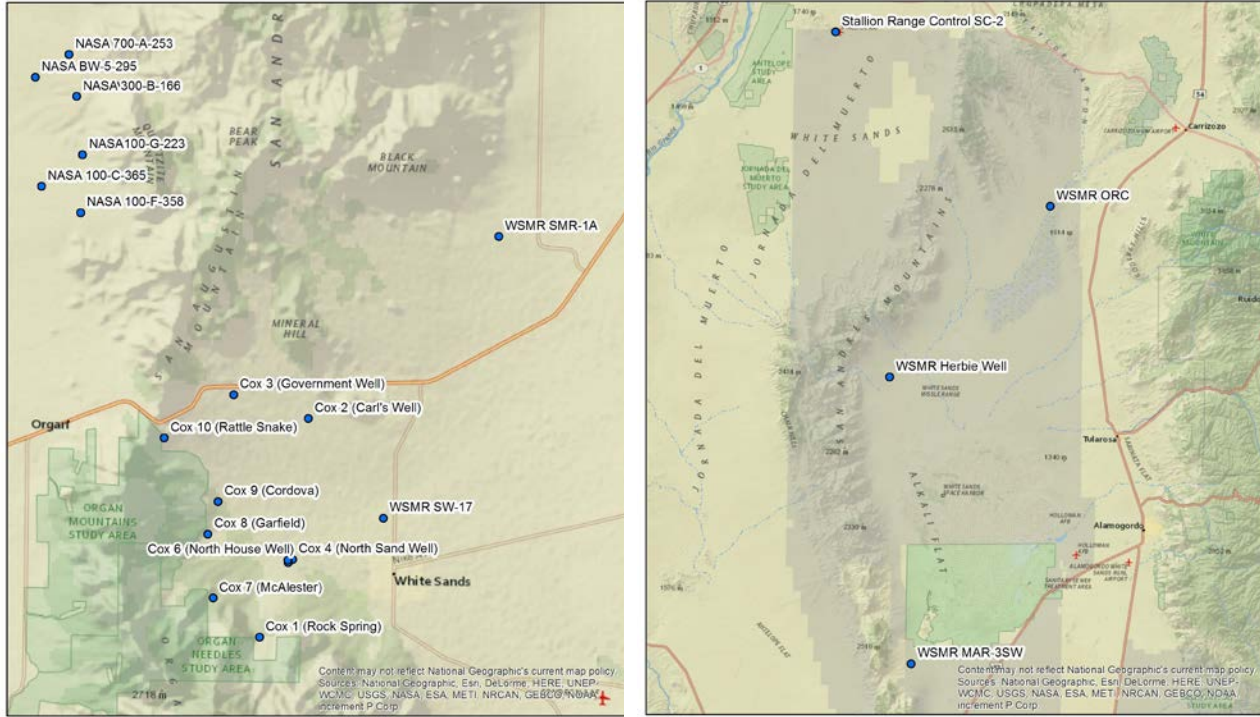
Figure 3. Wells sampled for water chemistry: WSMR main cantonment/ ADF-SW/NASA (left) and WSMR up-range (right).
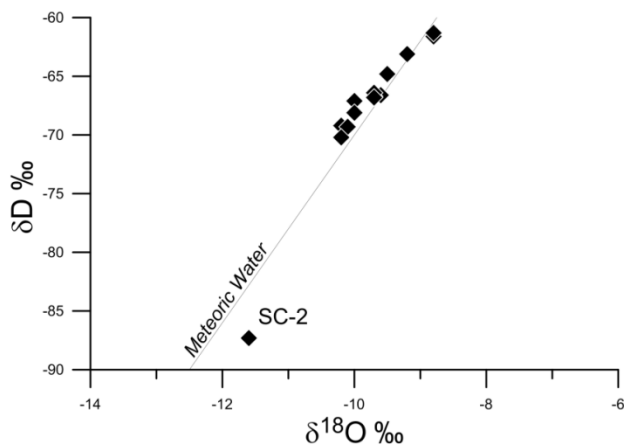

Figure 4. Hydrogen versus oxygen isotope values of groundwaters compared to the global meteoric water line. Their coincidence indicates that groundwater comes from local rain and snowmelt.
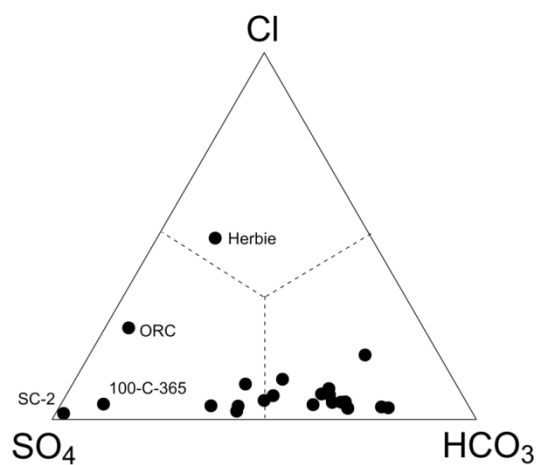

Figure 5 (right). Cl-HCO$_3$-SO$_4$ ternary plot, showing the predominance of bicarbonate in samples.

The Na-Ca-Mg ternary plot (Fig. 6) shows that most of the waters are rich in calcium, with the exception of BW-5-295 and 100-C-365, which are dominated by sodium. The absolute concentrations of calcium and magnesium range from 30-570 mg/kg and 5-175 mg/kg, respectively, and the co-variation in results plot in a rough linear trend (Fig. 7). Such high calcium and magnesium concentrations are unusual for

thermal waters, and like the stable isotope data, there is no strong evidence that any of the waters were subjected to high-temperature water-rock interaction.

As for geothermometry, the most reliable values are based on the concentrations of aqueous silica (10-50 mg/kg), which when compared to quartz-SiO_2 solubility (Fournier, 1991). These suggest equilibration temperatures in the range from 40 to 100 °C (Fig. 8). The quartz-SiO_2 geothermometer has broad applicability that includes low to high temperature resources that are hosted by a diverse range of rock types. By contrast, the K-Mg geothermometer yields cooler equilibration temperatures, whereas the Na-K geothermometer yields much hotter equilibration temperatures, but these calculated values are likely to be less reliable, given the high concentrations of aqueous calcium and magnesium. The quartz geothermometers were added to the existing PFA dataset and used for the development of the revised heat composite risk segment.

Well samples MAR-3SW, SC-2, SMR-1A and SW-17 have the hottest measured temperatures of ~25°C, whereas their quartz-SiO_2 equilibration temperatures are in the range of 70-90°C (Fig. 9). The physical and chemical measurements suggest that areas in the vicinity of these wells may be promising sites for future investigation. Sundance Engineering (2015) reports Well SW-17 as having a CO_2-N_2 geothermometer of 127.8 °C.

2.0.3 2m Temperature Surveys

These surveys were done by the Navy Geothermal Program Office (GPO). Data were collected over parts of ADF-SW/NASA and WSMR plays. The specific type of deployment used for this survey has been applied previously by the University of Nevada Reno's GBCGE and the Navy GPO (Coolbaugh et al., 2007, Sladek et al., 2007, Kratt et al., 2010, Lazaro et al., 2011, Skord et al., 2011).
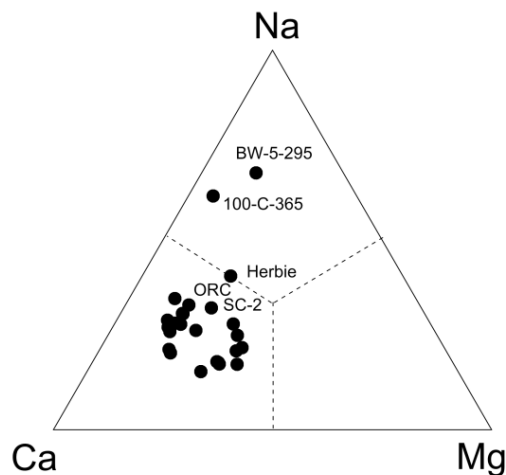

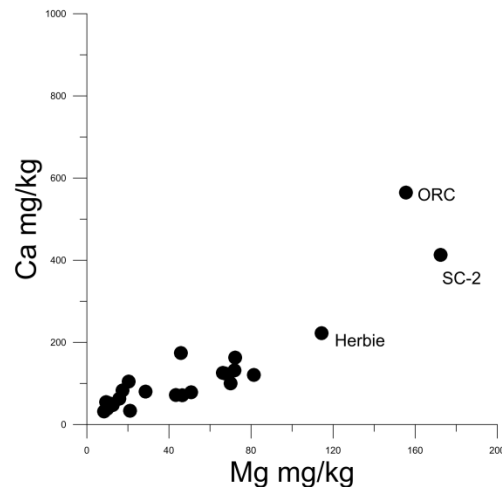**Figure 6. Na-Ca-Mg ternary plot, showing the predominance of calcium in samples.**

Figure 7. Calcium versus Mg concentrations in samples.

Figure 9. A comparison of calculated quartz-SiO2 solubility equilibration temperature versus measured field sampling temperatures.
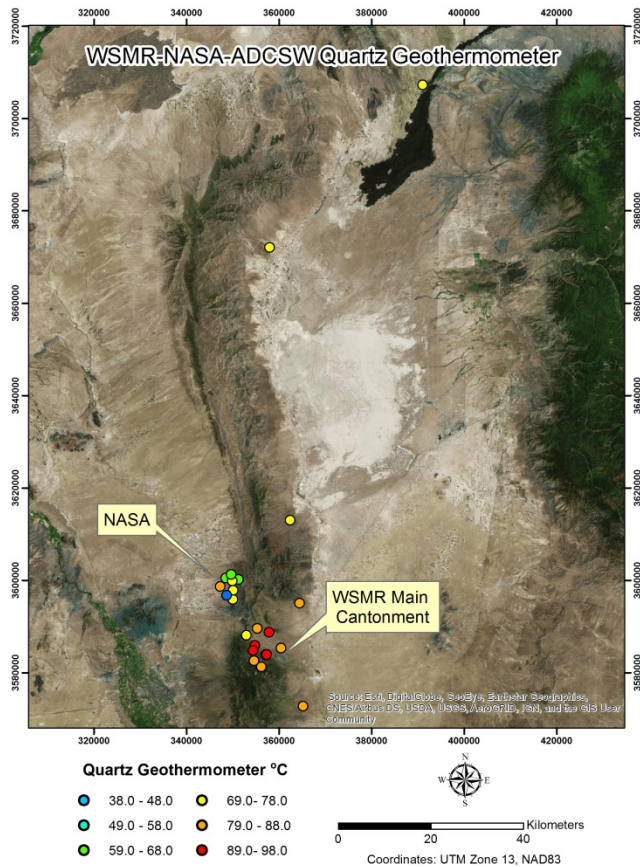

Figure 8. Quartz geothermometer results.

The GPO collected thirty-eight 2m probe points at ADF-SW/NASA between December 8th and December 11th, 2016 (Fig. 9). The data were collected by driving a 5/8" diameter, 2 meter long, hollow probe into the ground using a pneumatic hammer. A thermistor was then inserted down the probe and left to equilibrate for at least an hour before the shallow temperature was read and recorded. All of the points were accessed using either a truck or side by side ATV via existing roads. From January 6th through the 10th, ninety-one points were collected at WSMR employing the same methodology (Fig. 10). Both areas had locations with very shallow bedrock (usually ~0.25 meters depth) where the probe could not be installed. This is the reason for uneven spacing in some locations between points at both survey sites.

Base stations were established at both sites to facilitate temperature measurements throughout the duration of the survey that can be used to correct for seasonal changes. If more 2m probes are collected at these two plays in the future, these same base stations should be re-occupied to ensure consistent seasonal corrections in the data.

2.0.3.1 Base Station Correction

Base stations were located in the middle of each survey for ease of access (Fig. 10). For both base stations, the same thermistor was used to be consistent across both surveys. Base station readings were collected at the beginning of each day, in the middle of each day, and at the end of each day. These data were used to determine a seasonal bias by taking an average for the base station at each time interval; morning (AVG_{BM}), day (AVG_{BD}), night (AVG_{BN}). This value was then added to each base measurement to calculate a correction value ($Corr_{BM}$). This correction was applied to each 2m probe measurement (2m
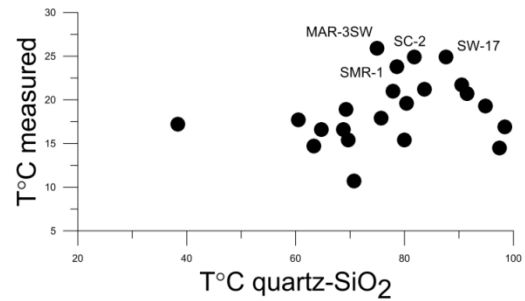
PM) to correct for a seasonal bias. AVG_B varied per day, time of day and per depth measurement (1m, 1.5m and 2m).

$$\text{Base station average: } (Base_M + Base_M + Base_M)/3 = AVG_{BM}$$
$$\text{Correction coefficient: } AVG_{BM} + Base_M = Corr_{BM}$$
$$\text{Corrected value: } Corr_{BM} + 2m\ PM = Corr2mProbe$$
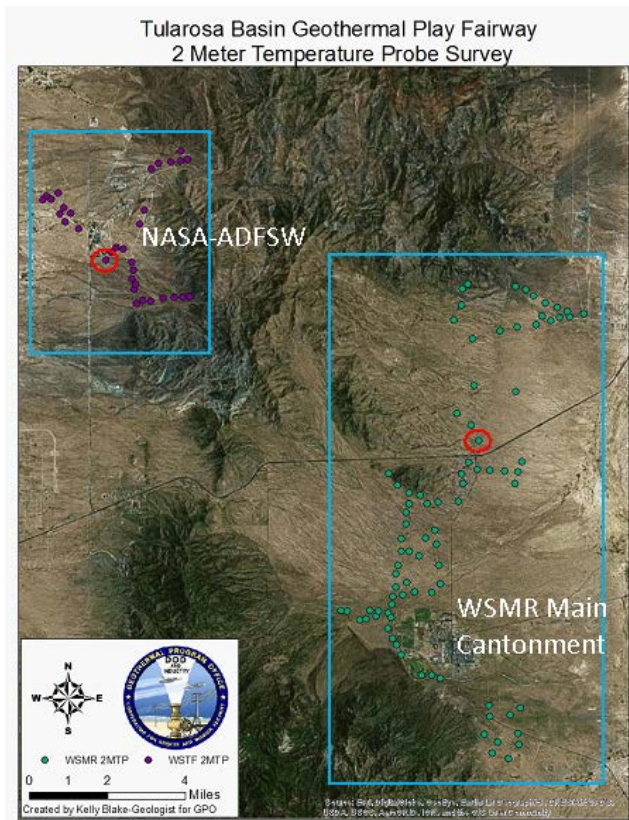

Figure 10. 2m probe points collected during December, 2016 and January, 2017. The purple dots are the points on ADF-SW/NASA and the green dots are the points on WSMR. The base stations are circled in red. The blue boxes represent the areas in Figures 3 and 4.

Thermistor Calibration and Correction

All thermistors were calibrated prior to deployment. Using a hot plate and distilled water in the GPO wet lab. Thermistor 1(T1) was used to determine the temperature of the heated distilled water. Every other thermistor (e.g., TX where X is the number of the thermistor) was then placed in the heated distilled water to measure temperature. The measured temperature of each thermistor (TX) was then subtracted from T1 to determine a corrected value (TX_{CORR}) for each thermistor. This thermistor correction was applied to every measurement. The thermistor correction (TX_{CORR}) was added to the base station corrections (Corr2mProbe) to yield thermistor calibrated and corrected temperatures (Corr2mProbeTX).

$$T1 - TX = TX_{CORR}$$
$$TX_{CORR} + Corr2mProbe = Corr2mProbeTX$$

2.0.3.2 Albedo and Topographic Slope Aspect Correction

Both the albedo of the surface and the ground slope where the probe measurement is taken are known to influence shallow ground temperature measurements (Sladek et al., 2009, Coolbaugh et al., 2010).

ASTER (Advanced Spaceborne Thermal Emmision and Reflection) imagery and Digital Elevation Model (DEM) data are used to correct for albedo and slope, respectively. For this survey, however, neither was found to have an effect on the data so these corrections were not applied.

2.0.3.3 RESULTS

After data corrections were performed, the values of Corr2mProbeTX for 1meter, 1.5 meters and 2 meters were used to create statistical surfaces using the natural neighbor method in ArcGIS (Figs. 11 and 12). Contoured 2m probe measurements at WSMR illustrate several clusters of high and low temperatures and a broad north to south alignment in the central and western margin of the investigated region (Fig. 11). The highest temperature Quartz geothermometers are just outside of the survey area; however, the 2 meter data contours vector toward these high values in the southwestern area of the survey.

At all three depths, the higher temperature anomaly follows the mapped Quaternary fault. There also seems to be a spreading out of temperature that begins where the western bend in the mapped fault occurs. This area is also very sandy. The larger area of anomalous high temperatures may be a product of structure and lithology.

At the ADFSW/NASA, the maximum temperature at 2 meters depth is about one degree Fahrenheit warmer than at WSMR. In Fig. 12, the 1 meter, 1.5 meter and 2 meter temperature contours and quartz geothermometer temperatures are mapped. There are no previously mapped Quaternary faults in this area. In the 1 meter temperature map, the anomalous high temperatures are along the range front. There is also a higher temperature lineation striking northwest from the southern extent of the survey. The 1.5 meter temperatures are warmer across the entire area. In the 2 meter temperature data, the hotter areas are more concentrated to the southern extent of the survey and along the northwest trend seen in the 1 meter data. At all three depths, a patch of anomalous temperatures were found in the western area of the survey, which coincides with the hottest quart geothermometer.

These surveys were done to help determine if anomalous heat was present in local areas, but not used in the PFA, which covers a much larger area.
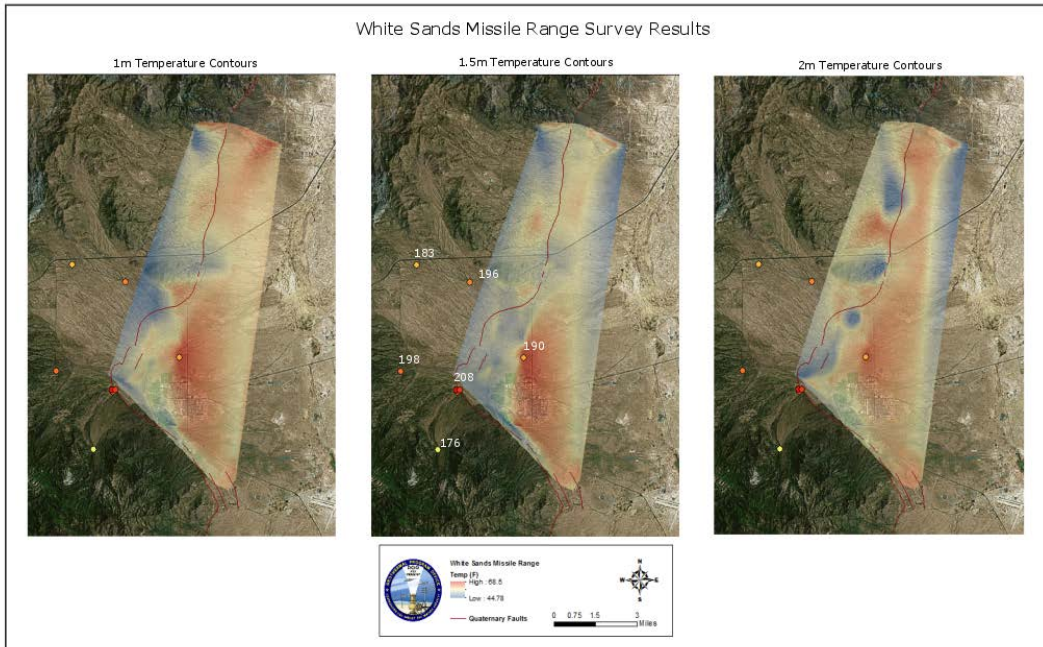
Figure 11. WSMR 2-meter temperature probe natural neighbor interpolation for 1m, 1.5m, and 2 depths. Quartz geothermometer temps are given in Fahrenheit on the 1.5 meter map (^{o}F). Red indicates higher temps and blue lower temps.
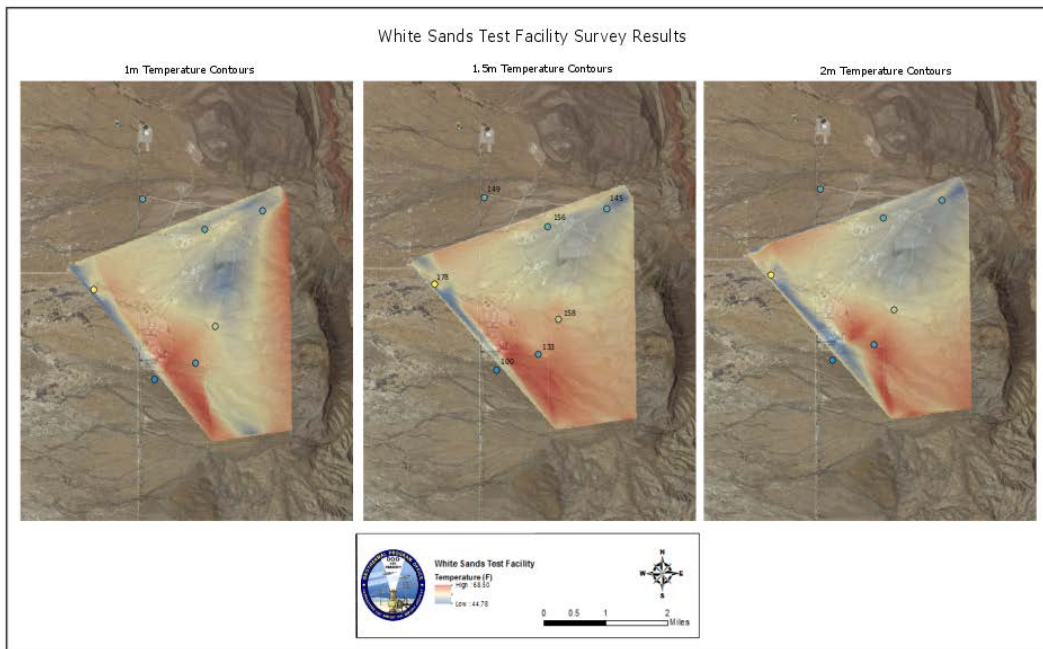

Figure 12. Natural neighbor interpolation for ADFSW/NASA temperatures at 1m, 1.5m, and 2m depths. Quartz geothermometer temperatures are labeled in the 1.5 meter map (^{o}F). Red indicates higher temps and blue lower temps.

2.0.4 Temperature Logging in Existing Wells

Temperature-depth profiles were measured and recorded at four ADF-SW/NASA monitor wells and eight White Sands Missile Range (WSMR) wells (Fig. 13) of varying types using high-precision

temperature logging equipment. The logging gear consists of a thermister probe attached to a reel-mounted, four-conductor, cable. Measurement accuracy is ±0.01°C. Because the probe equilibrates quickly in the water column, temperatures were measured at 2 m intervals in these zones. In contrast, measurements made above the water column take much longer due to slow equilibration times, and can be affected by
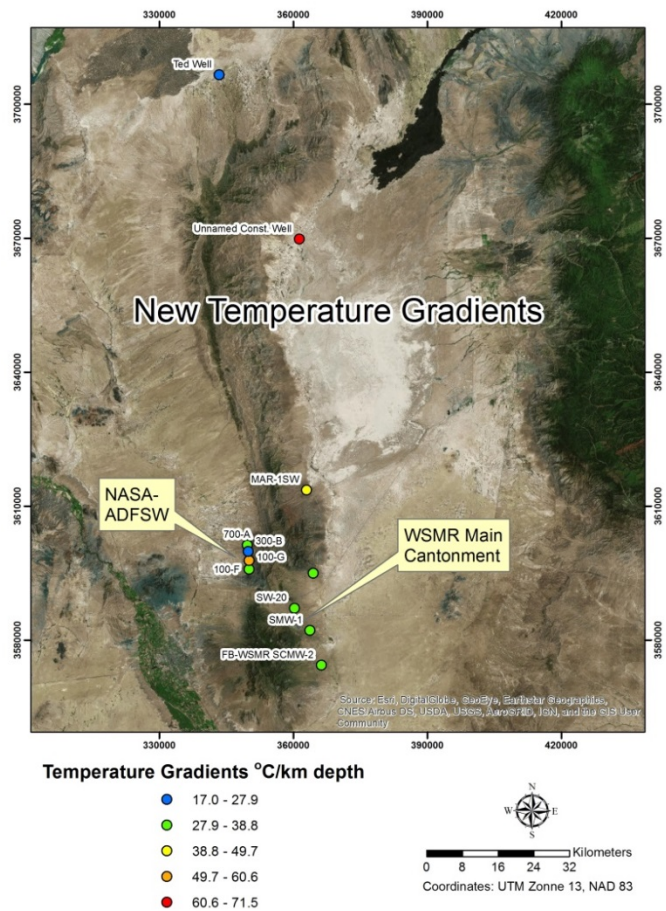

Figure 13. Temperature gradient results from existing wells.

transient air currents, especially near the top of the well, that diminish accuracy. Therefore, measurements in the air column were taken at coarser intervals (typically 5-25 m), depending on depth to water and the time available for logging a given well.

The ADF-SW/NASA monitor wells are pumped occasionally using low-volume pumps to obtain water samples, but none had been pumped for at least several weeks prior to temperature logging. The pumps in these wells were carefully removed to minimize disturbance of the static water and air columns that might affect temperature measurements. These wells were then left static for several days to re-equilibrate from any disturbance caused by removing the pumps. Therefore, it was assumed that all the wells were at static formation temperatures when logged. The pumps were reinstalled after logging and water samples were taken for geothermal analysis. Well depths ranged from 54.9 to 115.3 m. The profiles in these wells appear to be primarily conductive in nature and are generally similar (Fig. 14). Gradients from the linear segments at the bottom of each well range from about 22°C/km (well 300-B-166) to 59°C/km (well 100-G-223). Multiplying typical thermal conductivity values for the reported

lithology at the bottom of each well suggests that heat flow is lowest in well 300-B-166 (40 mW/m^2) and highest in well 100-G-223 (100 mW/m^2). Heat flow values for wells 700-A-253 and 100-F-358 are approximately 70 and 90 mW/m^2 respectively. However, thermal conductivity can vary greatly, so the uncertainty in these heat flow estimates may be on the order of ±20% or more. The reason for the much lower heat flow in well 300-B-166 is unclear, but could be related to cooler groundwater flow or greater uncertainties in thermal conductivity estimates or reported lithologies.

The WSMR wells consisted of monitor wells, primary water supply wells that are normally pumped, but had the pumps removed for maintenance/well rehabilitation, abandoned supply wells used for construction projects, and a supply test well. Most of these wells can be considered as "wells of opportunity" and were logged based more on accessibility than location. Locations ranged from south of the main WSMR cantonment to the Stallion Range Control area in the northern part of the WSMR range. A number of additional wells were checked for logging suitability that could not be logged for various
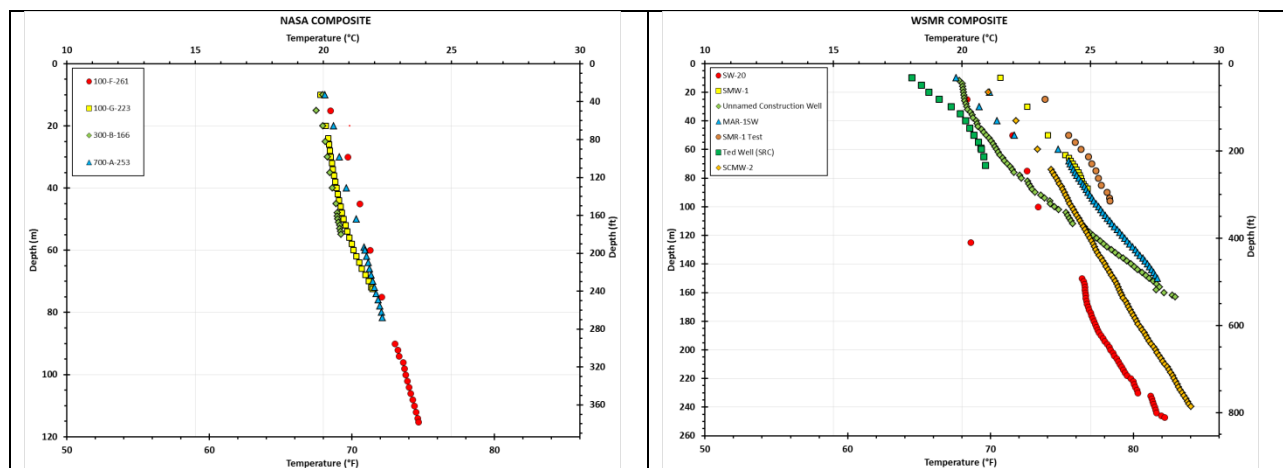

Figure 14 . ADF-SW/NASA (left) and WSMR (right) temperature log composites.

reasons. As far as could be determined, all of the wells had been static for quite some time and were assumed to be at thermal equilibrium. However, it is possible that pumping the SMR-1 supply well about 35 m from the logged SMR-1 Test well could cause a thermal disturbance. Unlike the ADF-SW/NASA wells, pumps are not installed in the WSMR monitor wells that were logged, so there were no issues with disturbing the wells prior to logging. Sample intervals varied in the same way and for the same reasons as in the WSTF wells. The temperature-depth plots are much more varied than those of the WST wells (Fig. 14). Profiles for all of the wells appear to be primarily conductive. An apparent equipment malfunction near the bottom of SW-20 is likely responsible for a small positive shift. These data were added to the PFA dataset and used for the heat CRS.

2.0.5 Gravity Data Acquisition & Analysis
A gravity survey was conducted by the Utah Geological Survey (UGS) in the Tularosa, New Mexico study area to delineate basement/subsurface structures. A total of 189 new gravity stations (Fig. 15) were acquired during the 2016 field season. Field measurements were made using a Scintrex CG-5 Autograv (precision of 1 µGal, accuracy of 5 µGal) following the methods of Gettings and others (2008) and using an absolute gravity base station located near Salt Lake City. Elevation control was established through post-processing of data collected by Trimble GeoXH GPS equipment for a minimum duration of 10 minutes and processed using Pathfinder Office Software tied to local CORS GPS base stations. We report

better than 10 cm vertical accuracy for all stations. Based on the vertical gravity gradient (0.3086 mGal/m) this procedure results in a gravity accuracy of better than 0.03 mGal (30 μGal).

Initial processing of the gravity data was followed by the calculation of terrain corrections, the Complete Bouguer gravity anomaly (CBGA), the horizontal gravity gradient. Inner-zone terrain corrections (0 to 67 m) were calculated by hand based on field terrain surveys using the methods of Gettings(2017). Outer-zone terrain corrections were computed using the methods of Gettings (2017) for each station from 67 m to 166.7 km using 90 m Shuttle Radar Topography Mission (SRTM) elevation data. CBGA values were computed using the methods outlined in Hinze et. al (2005). UGS gravity data were combined with legacy data from the Pan American Center for Earth and Environmental Studies (PACES, http://research.utep.edu/default.aspx?tabid=37229) to improve data coverage. Gravity anomaly and outer-zone terrain correction values were recalculated for the legacy data using the above methods before merging with newly collected UGS data. We conducted a gravity survey in the study area to delineate basement/subsurface structures.

Simplified 2D gravity model of a transect (Appendix B) in the study area was created using a variable thickness sedimentary layer overlying bedrock. The gravity anomaly values along the transect were adjusted for regional effects using low-order polynomials and subsequently modeled using the Semi-Automated Marquardt Inversion code (SAKI) of Webring (1985). The sediment and bedrock density contrasts were held constant for specific interval depths (for sediment layers) and based on estimated values from local geological information, samples, and drill logs of equivalent geographic areas containing sedimentary basins. A density-depth profile was developed using deep well data and densities were assigned in 500 m intervals for the basin fill as follows: 2.0, 2.16, 2.235, 2.31, 2.385, and 2.395 g/cm^3. Bedrock unit for the Tularosa study area was assigned a density value of 2.67 g/cm^3.

Bedrock outcrops on the margins of the valley and interpretations from geologic maps were used as depth-to-bedrock control points for the model to check layer density picks. The profile shows asymmetric basin comprised of a more steeply-dipping interface on the west side of the valley compared to more gently-dipping interfaces on the east side. The basin fill thickness at this location is estimated at a maximum just shy of 1.6 km near the center of the cross-section where the maximum gravity signal is approximately 27 m/Gal. Further north, the gravity anomaly signal is larger indicating sediments are potentially thicker. On the east side of the Organ mountains the gravity anomaly shows the start of a similar signal amplitude in the Tularosa Basin. However, accurate measurements would be required further to the east in order to constrain the Tularosa basin anomaly and have better controls for a future basin model.

Figure 16 below shows study area faults. A prominent Quaternary fault scarp is found curving through the WSMR main cantonment and then running north. Most of the other faults shown in this figure were interpreted from the gravity data.
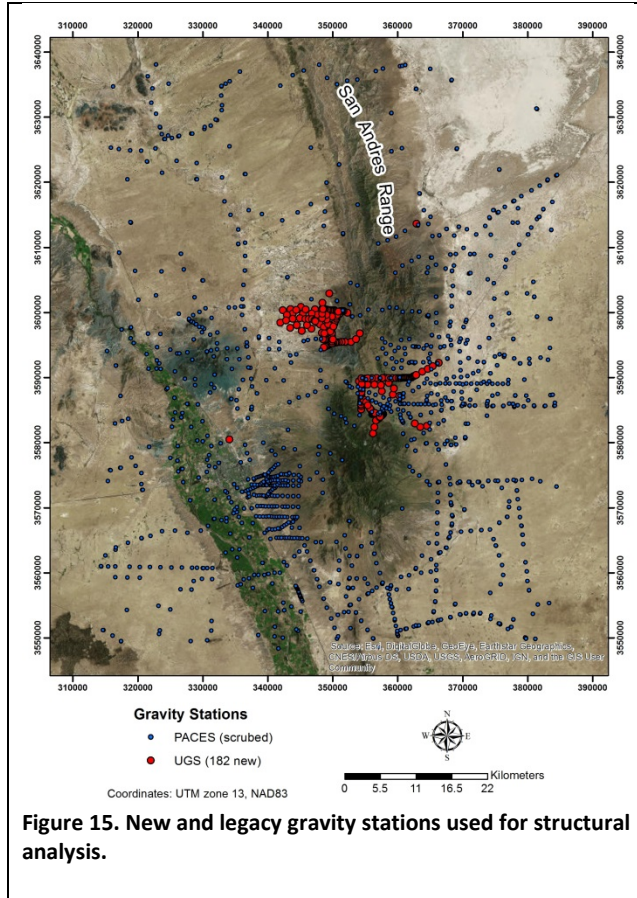
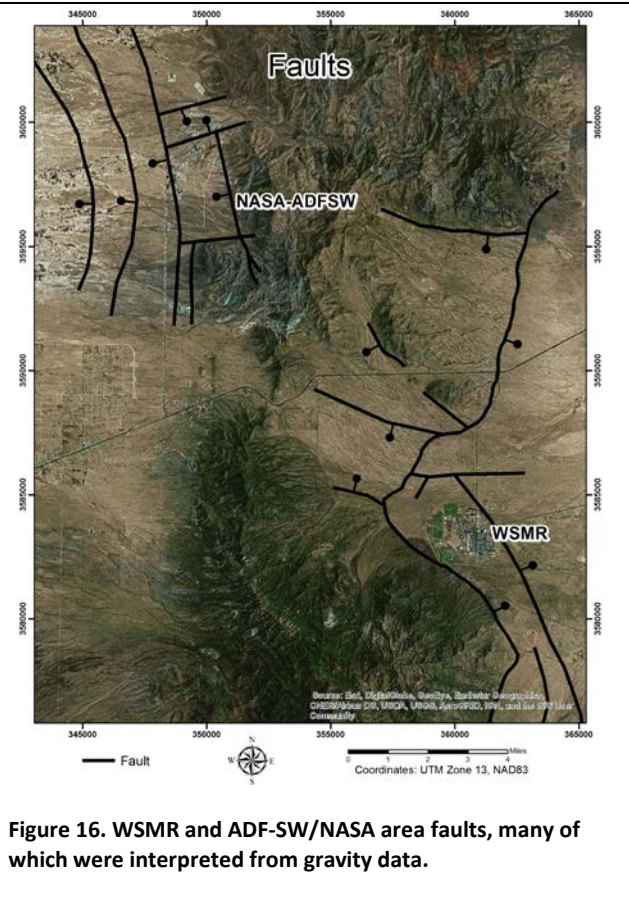**Figure 15. New and legacy gravity stations used for structural analysis.**

Figure 16. WSMR and ADF-SW/NASA area faults, many of which were interpreted from gravity data.

2.0.6 Magnetotelluric Survey: McGregor Range

A magnetotelluric (MT) survey was done at McGregor Range on Fort Bliss, to help better characterize the area of validation well 56-5, which was drilled by Ruby Mountain Inc. under a DOE ARRA grant. Well 56-5 showed good promise during drilling when several hot water entries were encountered. This well will be flow-tested toward the end of this project, and if adequate flow is achieved, a 0.25 MWe test plant will be installed. The MT survey was run looking forward to the possibility of future development and the potential need to site additional production wells.

To this end, a 56 station survey was conducted by Quantec Geoscience during January, 2017. The data were then submitted to EGI where inversion modelling was accomplished. This is detailed in Appendix B. We interpret this data as showing a NW trending conductor that may be related to hydrothermal alteration on a mapped Quaternary fault. This system was not well understood prior to this survey and may be a target for future drilling (Fig. 17).
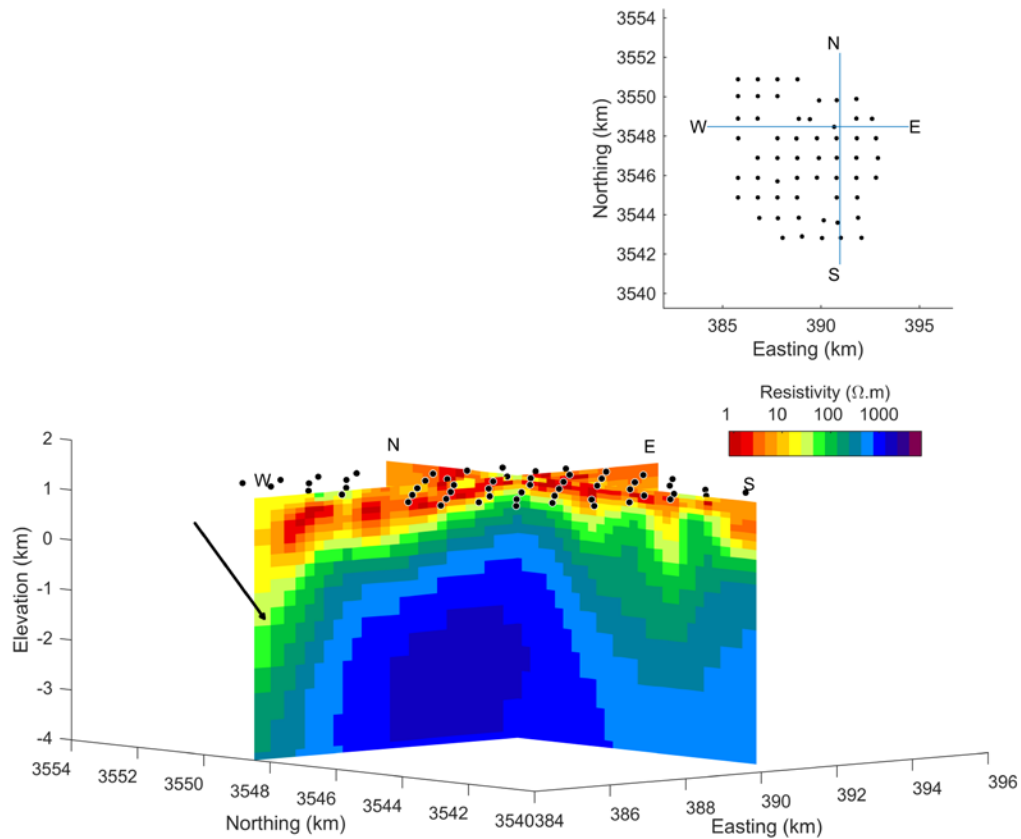
Figure 17. A conductive zone, indicated by the arrow, is believed to be a Quaternary fault system that may be a source of geothermal fluid and a target for future drilling.

3.0 PFA Model Development

Our Phase 1 Play Fairway Analyses (PFA) used a deterministic method based upon petroleum industry logic (Fraser et al., 2001) and the probabilistic Weights of Evidence method (Sawatzky et al, 2009; Coolbaugh, 2003; Bonham-Carter, 1994). The models were based upon (1) the heat of the Earth, (2) fault related fracture permeability, and (3) the presence of ground water. The heat and water data used in these models was collected from public databases, local governments, and literature. Upon exhausting these sources, enough data was present to create the PFAs, although significant expanses of the study area were data poor or devoid of data. Fault related fracture permeability was considered to be areas along and adjacent to Quaternary fault systems and areas of critical stress (Faulds et al., 2006, 2010, 2013). Zones of critical stress were mapped using geomorphological characteristics along with gravity and aeromagnetic data interpretation. Phase 1 PFA analyses identified 12 plays (Fig. 18). The plays were then prioritized based upon economic analyses, land status, and proximity to transmission lines. Phase 2 PFA models were developed in a generally similar manner. However, new data acquired as part of this project were added.

3.0.1 Phase 2 Deterministic Play Fairway Analysis: Petroleum Logic Approach

3.0.1.1 Heat of the Earth CRS

The methods used in Phase 2 closely follow those detailed in our Phase 1 report, with the notable exception that in Phase 1 the 2011 SMU Geothermal Laboratory Heat Flow Map of the Coterminous United States (Blackwell et al., 2011) was used for heat flow. For Phase 2, this data was thought to be overly generalized due to the small scale of the map. Therefore, the SMU Geothermal Laboratory heat flow data were re-interpolated over the study area. Additionally, new quartz geothermeters and temperature gradient data, acquired during Phase 2, were added to Phase 1 datasets which were re-interpolated. All data locations can be viewed in Fig. 19. The resultant raster grids were then classified as follows and vectorized as discussed in detail in our Phase 1 report.

Temperature gradients: 0 ^{o}C/km – 60 ^{o}C/km = High Risk; 60 ^{o}C/km – 80 ^{o}C/km = Medium Risk; >80 ^{o}C/km = Low Risk

Quartz Geothermometer: 0 ^{o}C – 60 ^{o}C = High Risk; 60 ^{o}C – 80 ^{o}C = Medium Risk; >80 ^{o}C = Low Risk

Heat flow was digitized as vector data directly from the SMU 2011 heat flow map (Blackwell et al., 2011). It was classified as follows (mW/m^2): 55 – 70 = High Risk; 70 – 85 = Medium Risk >85 = Low Risk

The final heat CRS was then created through the fusion of the three heat vector layers. The results can be observed on (Fig. 20).

3.1.2 Fracture Permeability CRS

This CRS was developed using Quaternary faults and zones of critical stress (Fig. 21) (Faulds et al., 2006, 2010, 2013). Quaternary faults were derived from the USGS Quaternary Fault and Fold Database of the United States. These data were clipped to fit the study area and then buffered at a distance of 1 km. The resultant polygons were then all classified as Medium Risk. Quaternary faults and recent seismic actively are known to be related to permeability in geothermal systems, but fault slippage can both open and
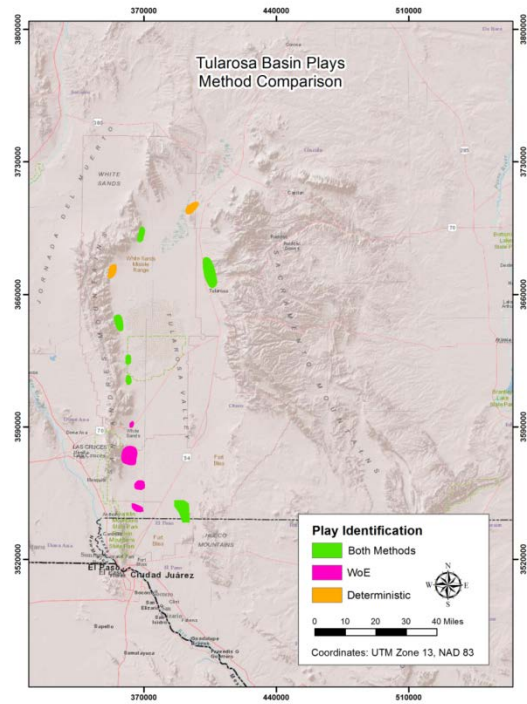
Figure 18. Plays identified in Phase 1 and a comparison of the methods which identified them.
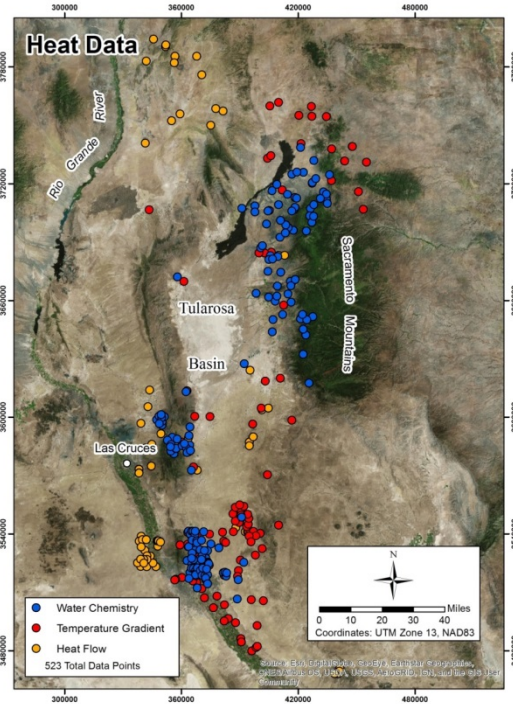

Figure 19. Datasets representing the heat of the Earth. Note that the data types are generally spatially separate.
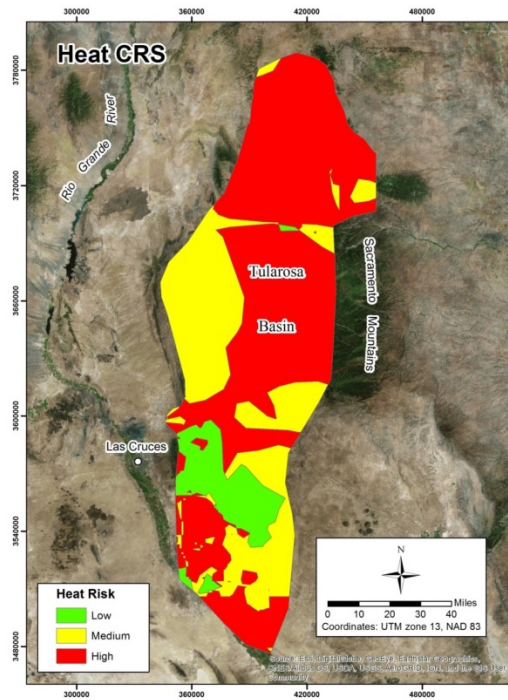

Figure 20. Heat CRS: fusion of heat flow, temperature gradient, and quartz conditional geothermometer data.
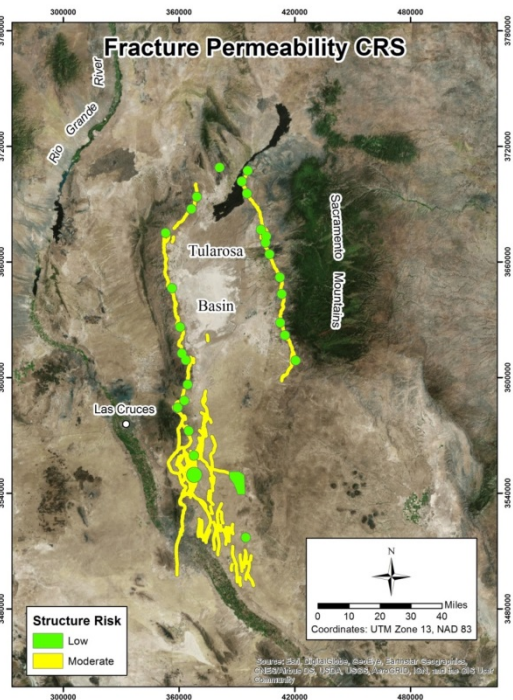

Figure 21. Fracture permeability CRS: Quaternary faults @ 1 km buffer (each side of fault) and 5 km diameter zones of critical stress. Areas within the study area that are not colored are high risk.

close fractures. Therefore, we believed that Quaternary faults needed to be represented, but not as Low Risk. Zones of critical stress form in structural settings such as fault step-overs, tips, apexes, intersections, ramp relays, and accommodation zones. Critical stress zones were mapped using aerial photography, Bouguer gravity, and total magnetic data interpretation. Each zone was considered to be encompassed within a 5 km diameter buffer circle, except where evidence indicated that a larger area may be impacted. Resultant polygons were classified as Low Risk (Fig. 21).

3.0.1.3 Ground Water CRS

Ground water appears to be well distributed in the Tularosa Basin based upon producing wells (New Mexico Office of the State Engineer – POD waters). Additionally, Pleistocene Lake Otero occupied the west central part of the basin providing deep aquifer recharge. There are also numerous water wells not found in the POD database located at WSMR and ADF-SW/NASA. It was found during Phase 1 that water was of little consequence in the PFA due to its availability. Therefore, the Phase 2 deterministic PFA did not use a ground water CRS.

3.0.1.4 Final Petroleum Industry Logic PFA

The final deterministic PFA was created through an overlay of the heat of the Earth and fracture permeability CRS layers (Fig. 22). This PFA contains 7 plays, whereas the Phase 1 PFA deterministic model that produced 8 plays. This was due to the re-interpolation of heat flow data, which eliminated some broadly interpolated high heat flow areas in the west-central and northwestern part of the basin.

3.0.1.5 Certainty

Certainty has many factors including data quality and spatial distribution. Because all of the data used in Phase 1, which also constitutes the majority of data used for Phase 2, came from public databases and literature, we can only assume that it is of high quality. The newly acquired data used in Phase 2 modeling were collected using best known industry practices.

Spatial distribution is critical due to inherent error which propagates between widely spaced data points during interpolation. Therefore, data points were buffered at a 5 km radius with the results being incorporated into the model to show areas of no data, which are low certainty (Fig 23.). This reduced the number of plays to six through the elimination of a play which was based solely upon interpolation. Simple kriging probability was also used, at a threshold of 0.8, for certainty as follows: 0.0-0.6 = low certainty, 0.6-0.8 = medium certainty and 0.8-1.0 = high certainty for heat CRS input data (Fig. 24). Only three plays fell into the high certainty category. The availability of water was also considered, although not as an input CRS, through an overlay shown in Fig. 25, which shows water within all low risk areas.

3.0.2 Stochastic Play Fairway Analysis: Weights of Evidence Approach

The weights of evidence (WoE) method used for the Phase 1 was again applied to the revised Phase 2 data. The use of this technique was based on work done by Moghaddam et al. (2013), where they found it to be the superior stochastic method, out of several tested, for geothermal exploration model development. This technique examines multiple layers of evidence, which makes it ideal for this work. It first calculates weights for each evidential layer based upon the spatial relationships of training points,
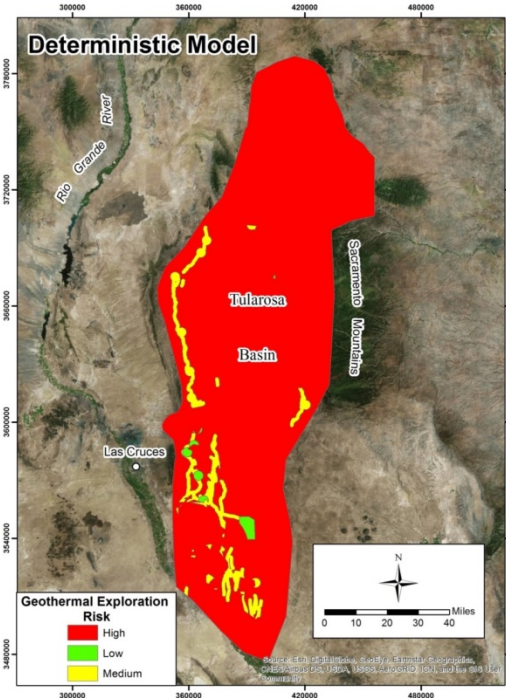
Figure 22. Deterministic petroleum industry logic PFA model suggesting seven potential plays.
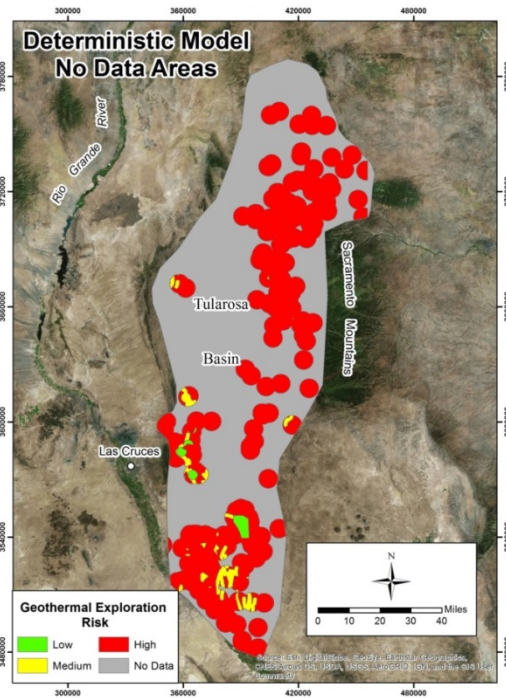

Figure 23. Areas of no data (gray) in relation to PFA results.
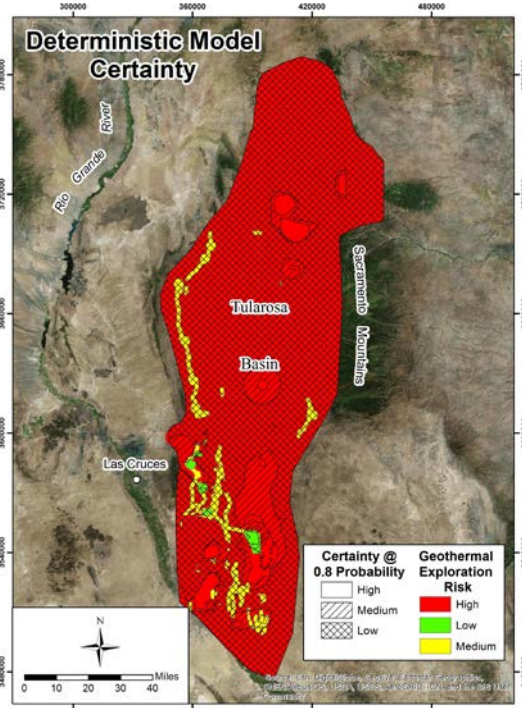

Figure 24. Certainty based upon a 0.8 cutoff on CRS simple kriging probability models.
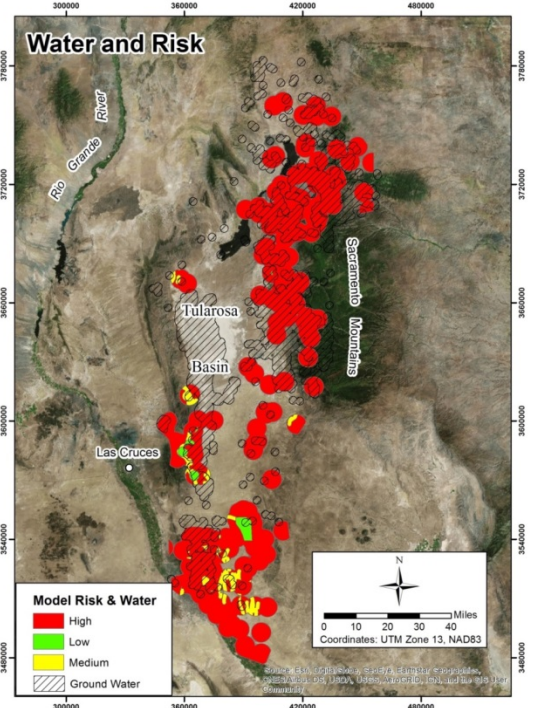

Figure 25. PFA with no data zones removed and the water resource layer added. Water is available within all low risk areas.

which are located at known geothermal systems and hot springs, and then produces a posterior probability raster surface, a certainty raster surface, and other related statistics.

A problem applying this method was encountered for the Tularosa Basin where a lack of training sites existed. There is only one partially proven geothermal system in the area and no hot springs exist. This was addressed by creating regional statistical surfaces, for training use, that covered Nevada, Utah, and New Mexico. This gave access to ample training sites. Spatial Data Modeler was used for the WoE analysis (Sawatzky et al., 2009).

3.0.2.1 WoE Layers of Evidence

In Phase 1, water chemistry data, from the Great Basin Groundwater Geochemical Database from the Nevada Bureau of Mining and Geology (http://www.nbmg.unr.edu/Geothermal/GeochemDatabase.html) and additional data from the Oregon Institute of Technology Geo-Heat Center (http://www.oit.edu/orec/geo-heat-center), were compiled into an ArcGIS shapefile. Redundant points were removed and the quartz (conductive) geothermometer (Fournier, 1991) calculated. The IDW interpolation method was then applied to the quartz geothermometers using ArcGIS to create a regional raster statistical surface. The same process was also applied to heat flow and temperature gradient data originating from the SMU Geothermal Laboratory (http://www.smu.edu/dedman/academics/programs/geothermallab). Extrapolation was allowed into areas with no data for the evidential layers. However, training sites were only chosen in data rich areas where the statistical surfaces were very accurate.

For Phase 2, raster IDW statistical surfaces, specific to the Tularosa Basin project area, created for the deterministic model using newly acquired data as well as data collected during Phase 1, were integrated onto the regional surfaces discussed above to update them (Fig. 26). The datasets were then classified, using standard deviations of the mean, to: Heat Flow = 16 classes, Temperature Gradients = 12 classes and Quartz Geothermometers = 13 classes).

Fault related fracture permeability was represented by zones of critical stress (Fig. 27). These originated from the Faulds Structural Inventory of Great Basin Geothermal Systems and Definition of Favorable Structural Settings (http://en.openei.org/datasets/dataset/structural-inventory-of-great-basin-geothermal-systems-and-definition-of-favorable-structural-setti2) for Nevada and Utah and were mapped by the PI in New Mexico. These data were considered to be binary (critical stress zone = 1, all other areas = 0) in the layer of evidence. Training points are shown in Fig. 28. Ground water was not used as a layer of evidence for the same reason given in the deterministic model section earlier in this report.

The final WoE post probability model overlain with the WoE confidence layer is shown in Fig. 29. It was not anticipated that high probabilities would be produced for the Tularosa Basin due to the placement of training points at known systems that were generally high enthalpy and this was the case. McGregor Range at Fort Bliss, the only know geothermal system in the area, had the highest probability within the study area.
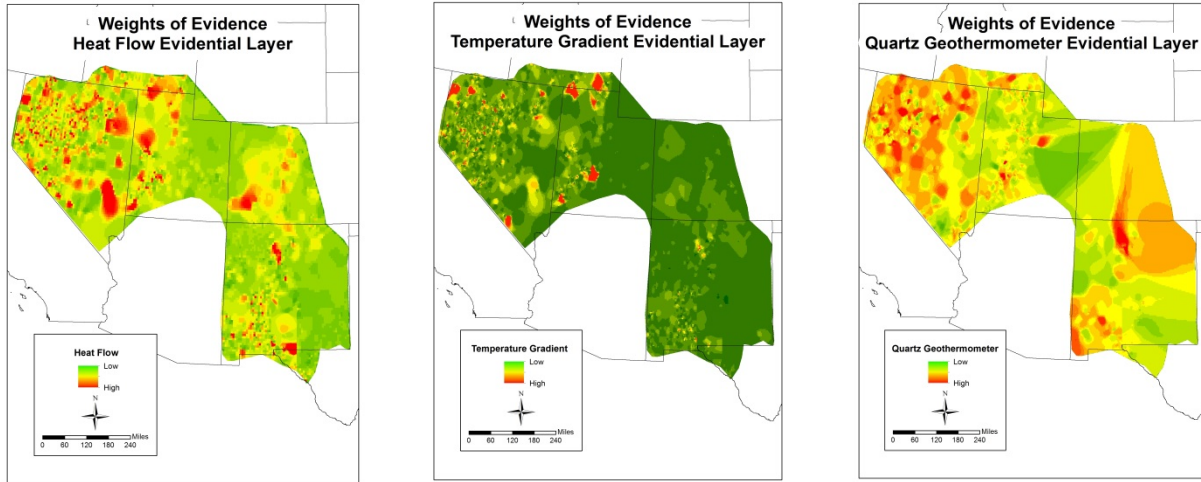
Figure 26. Evidential layers for heat. Please note that no data were used for eastern Utah or Colorado so data covering these areas are interpolations. Training points were located in data rich areas in Nevada, New Mexico, and Utah.
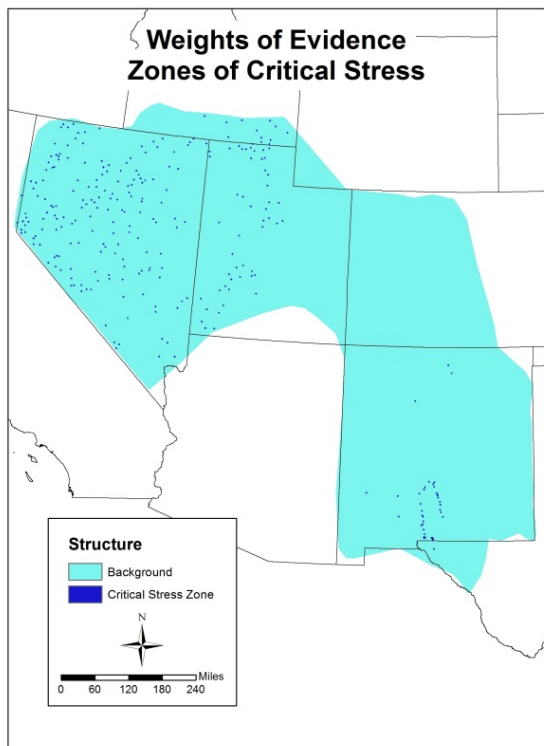

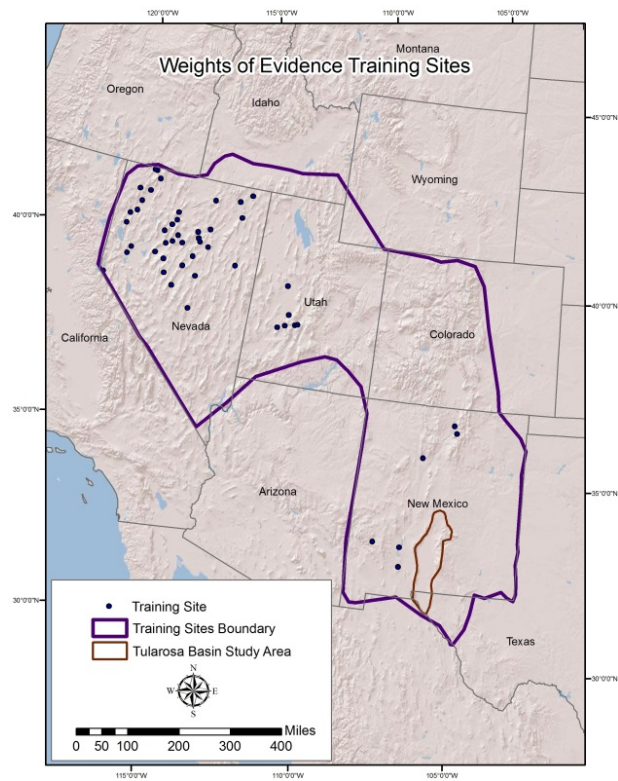**Figure 27 . Zones of critical stress layer of evidence.**

Figure 28. Training points used in WoE analysis.
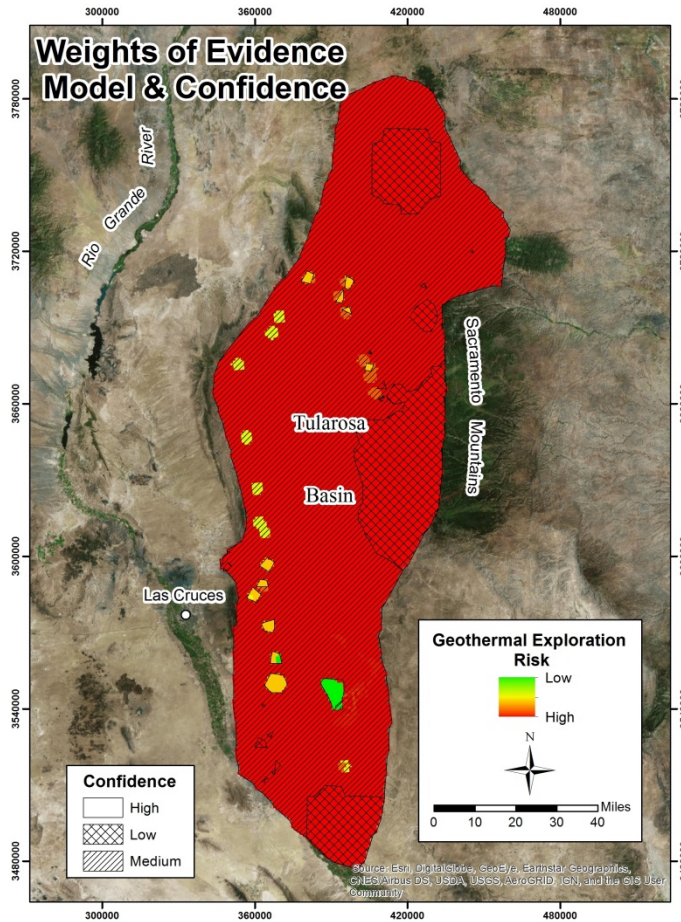
Figure 29. WoE post probability model overlain with the WoE confidence layer. Red areas have 0.0 probability. McGregor Range at Fort Bliss had the highest probability in the study area. It too, however, has the most available data.

3.0.3 Final Plays

Plays from the deterministic model were chosen primarily on being located in low risk areas. Plays from the WoE model were chosen primarily on having probability values that were greater than background. Certainty was then considered and a play had to have high certainty either from (1) kriging probability or (2) WoE confidence. Finally, each play had to be at least partially within a 5km radius of data. The final play map can be seen in Fig. 30.

Figure 30. Final Phase 2 play map showing the methods used to choose the plays. Most of the plays were chosen by both methods.

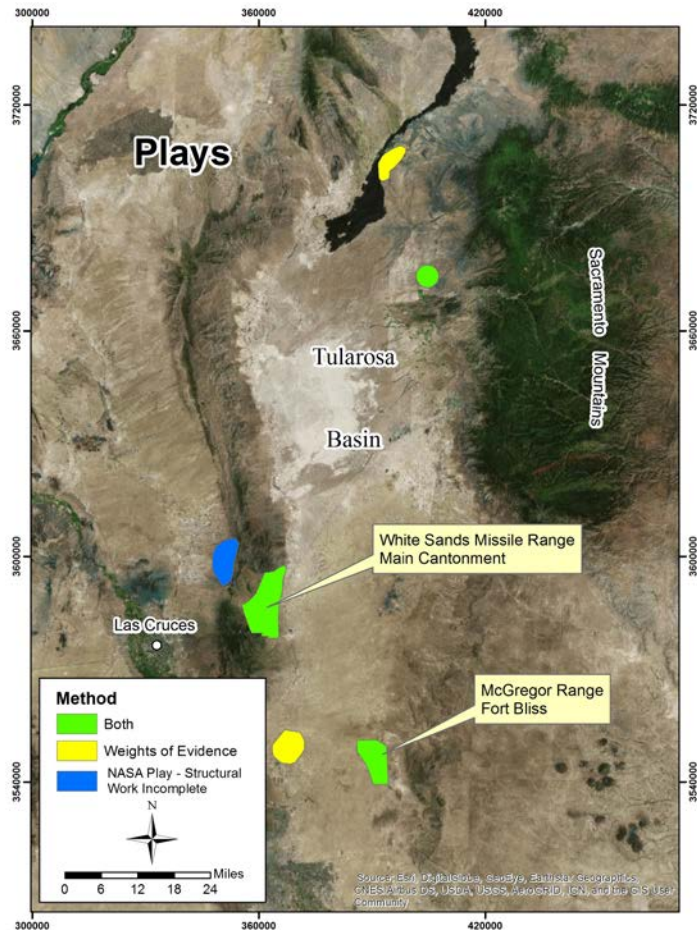Phase 2 resulted in a significantly reduced number of plays from those produced in Phase 1 (Fig. 31). This was in part due to the re-interpolation of heat flow data, as previously mentioned, which resulted in lower values over part of the study area and because of the application of certainty and areas of no data in a conservative manner. Additionally, the plays were prioritized (Fig. 32) as follows: (1) if both PFA methods indicated the presence of a play and all methods of certainty were high the play was considered high priority; (2) if both PFA methods indicated the presence of a play an only a single method of certainty was high, the play was considered medium priority; and (3) if a single PFA method indicated the presence of a play and a single method indicated high certainty the play was ranked as low priority. This leaves the McGregor Range and WSMR Main Cantonment plays as the highest priorities.

The ADF-SW/NASA play (colored blue on Figs. 30, 31 & 32) was in the low risk category on the deterministic heat CRS, however, no zone of critical stress in a Quaternary fault system has yet been positively identified and since quartz geothermometers suggest increasing heat toward the west part of the play further heat validation is warranted. This work at this play is funded by the U. S. Air Force. It is
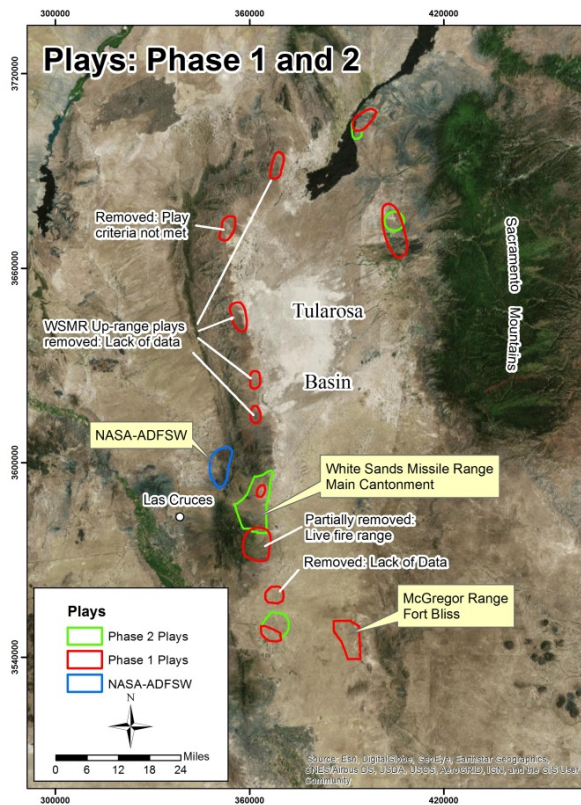
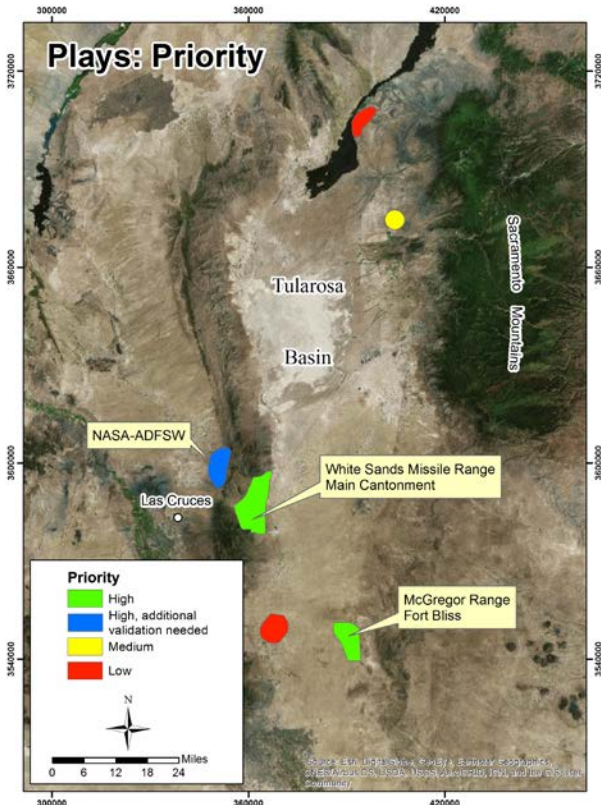**Figure 31. Play comparison between Phase 1 and Phase 2.**

Figure 32. Phase 2 play prioritization.

anticipated that additional data will become available to complete this work. If a zone of critical stress can be confirmed, it will become a PFA high priority play.

4.0 Conclusions

New data, collected during Phase 2, representing the heat of the Earth, in the high priority areas at WSMR and ADF-SW/NASA add evidence of geothermal systems. Quartz geothermometers in the WSMR Main Cantonment area suggest temperatures as high as 98 $^{\circ}$C (Fig. 8). Although data suggests significant ground water mixing, this is one of the highest quartz geothermometers found in the study area. Several nearby wells also have similar, but slightly lower, quartz geothermometers. This is unique within the study area where there are a few spotty similarly high values, but no other known clusters exist. In comparison, the geothermal validation well 56-5 at McGregor Range, Fort Bliss, has a quartz geothermometer of 94 $^{\circ}$C. Additionally, the shallow (2m) temperature survey at WSMR had a spatially correlative temperature anomaly projecting toward this cluster. The shallow temperature survey also exhibited temperature anomalies that correlated well with the Quaternary fault system and showed interesting clusters near the northern and southern extent of the survey (Fig. 33). Temperature logging of existing wells generally did not indicate high temperature gradients. This may be due to the influx of cold ground water. Unfortunately, the choice of wells for logging was generally based upon availability and the spatial relationship with the Quaternary fault system was not optimal. However, a gradient of 71.5 $^{\circ}$C/km was found at an unnamed construction well up-range at WSMR. This area did not become a
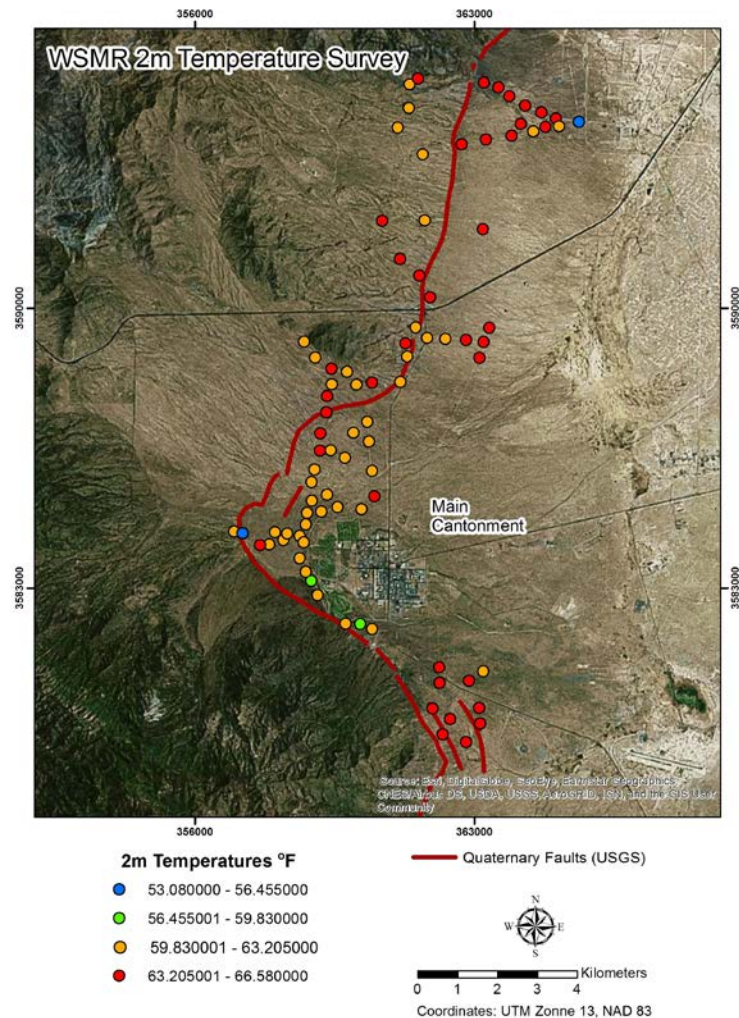
Figure 32. WSMR shallow temperature survey results.

play because this was lower than the allowed threshold. However, it is believed that more work may be warranted in this area in the future.

Structural interpretation from gravity data has provided new insights both at WSMR and ADF-SW/NASA. New faults have been interpreted including en echelon faults outboard of the range-fronts at ADF-SW/NASA at WSMR. Intersecting and interconnecting faults have also been mapped that may be creating zones of critical stress. This is especially prominent at WSMR where structural remnants of oroclinal bending likely influenced the propagation and linkage of the San Andres and Organ fault systems. Additionally, seismic profiles, provided by NASA, suggest that en echelon faults offset buried Quaternary sediments at ADF-SW/NASA, raising the stakes at this play.

Finally, while there is not 100% certainty that there is a geothermal system at any of the plays identified in our study, with the exception of McGregor Range, we believe that the probability has been significantly raised. The WSMR main cantonment area shows good promise. Therefore, we recommend drilling 1000' deep temperature gradient holes in this area for validation. The ADF-SW/NASA play is also beginning to show promise and we assume that additional funds will become available from the Air

Force to advance this area. Other areas in the Tularosa Basin may also have geothermal systems, such as the Rhodes Canyon play, where the unnamed construction well had a relatively high temperature gradient. Additionally, the geochemistry of wells MAR-3SW, SC-2, and SMR1A suggest the possibility of geothermal activity in their respective areas. However, data is sparse to nonexistent over much of the study area, but it is hoped that this study will provide information that will help guide future exploration.

5.0 Phase 3 Proposal

Both models used in our PFA have already identified the McGregor Range geothermal system (Play #1) on Fort Bliss which has been our top ranked play through Phases 1 and 2 and the play has been verified. Subsequently, Phase 3 field work will focus on further proving out the plays at WSMR (Play #2) and at ADF-SW/NASA (Play #3) – both of which have captured the military's interest for possible future development. See Fig. 33 below.

To round out our Phase 3 efforts, we propose to do some additional "ground truthing" at plays uprange at WSMR (Play #6) and on the western side of Fort Bliss (Play #5). No substantial work has been done in these areas due to budgetary constraints in previous project phases, however, both areas continue to be of interest to the team and could be significant in terms of providing additional verification to the PFA methodology. Both of those plays could also be of interest to the military in terms of future development, as modest amounts of reliable power are often needed in remote locations. See Fig. 33 below. No work is proposed at this point on Play #4 due to our inability to contact the private land owner who lives in Texas.

The bulk of our Phase 3 budget will focus on drilling up to 8 thermal gradient (TG) holes at WSMR. The holes as proposed will be 2" in diameter and approximately 1,000 ft. deep. The Navy GPO will log the holes before they are abandoned. We believe that the relatively shallow wells logged in Phase 2 generally had an influx of cooling ground water. In Phase 3 we plan on drilling deeper into solid rock beneath the cold water aquifer.

The second primary expenditure during Phase 3 will focus on magnetotelluric (MT) surveys at both WSMR and at ADF-SW/NASA. We believe that the MT data will help characterize structures and show faults with hydrothermal alteration where hydrothermal fluids have been mobile. We would also like to determine if clay caps exist in those areas.

Other, less costly field work will include:

Gravity infill to provide critical information on geologic structure and help determine zones of critically stressed rock where geothermal reservoir permeability may exist.

Shallow temperature surveys will be conducted in some new areas where critical stress is likely. This low-cost method can help affirm the presence of heat and the locations of hydrothermal up-flow and out-flow zones.

Water samples will be collected from up to 14 additional wells in the area for chemical analysis and geothermometry. Down-hole temperatures will be logged from those wells to improve the temperature gradient database.
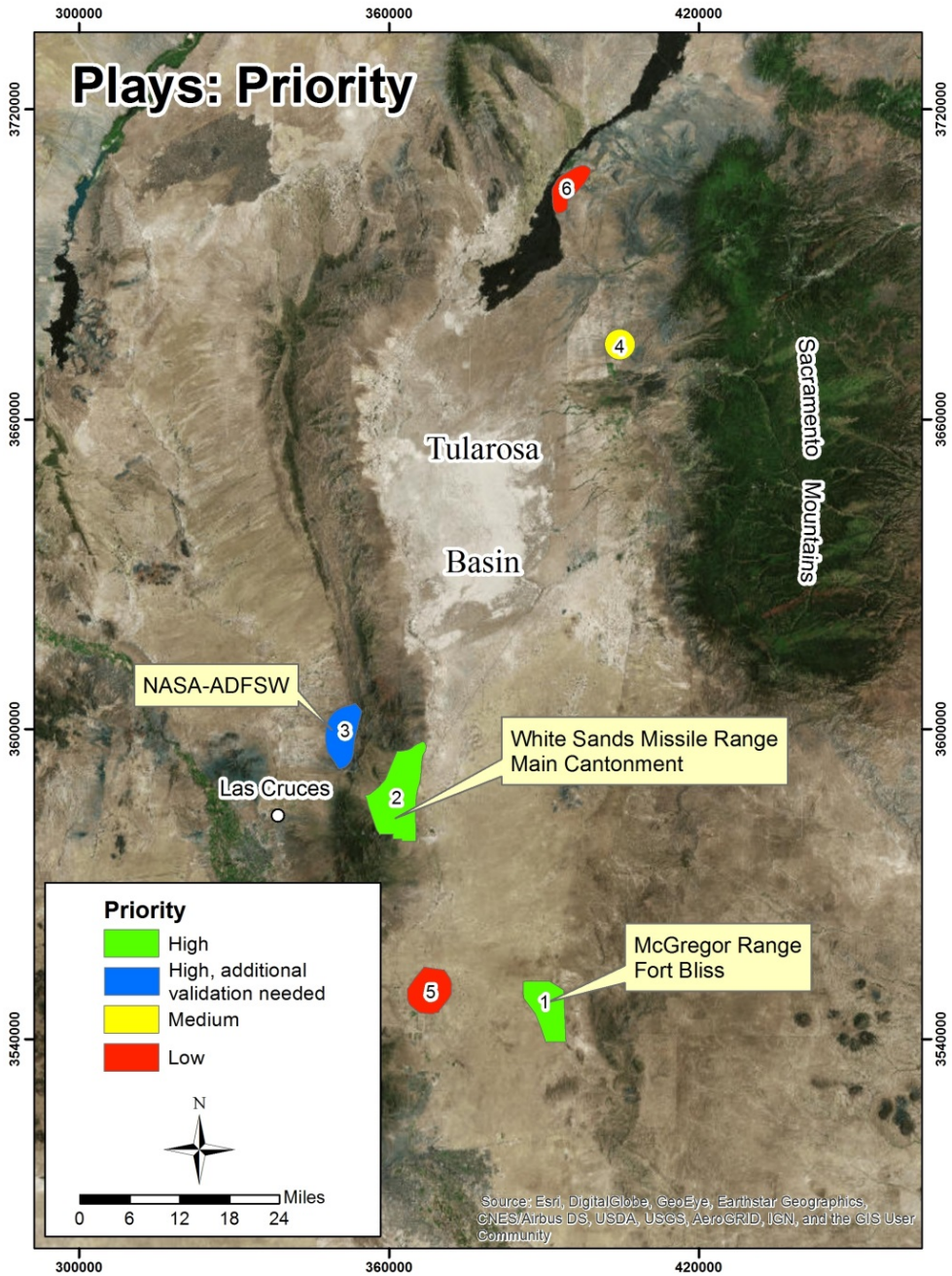
Figure 33. Ranked plays following Phase 2.

Specifically, the following work will be done at each Play and will be funded through a combination of DOE, Ruby Mountain/EGI funds and from an anticipated Phase 3 ADF-SW contribution.

Play #1 – Fort Bliss' McGregor Range – HIGHEST PRIORITY PLAY
PLAY VERIFIED – No Phase 3 Work proposed for funding by DOE. However, Ruby Mountain will fund an economic evaluation of the play for U.S. DoD/Fort Bliss in order to help encourage development of the resource.

Play #2 – WSMR Main Cantonment – HIGH PRIORITY PLAY
1. Additional gravity infill (50-70) stations
2. 8 Temperature gradient holes approx. 1,000 ft. deep and 2" diameter
3. Logging of TG holes
   -- Go/No Go Decision --
4. MT Survey (80-120 stations)
5. Development of a 3D geothermal system model
6. Siting of deep resource confirmation well(s) for future drilling by DoD

Play #3 – ADF-SW/NASA – HIGH PRIORITY PLAY
1. Water sample collection in expanded study area for chemistry and geothermometry; logging
2. Expanded shallow temperature survey (45-55 stations)
3. Additional gravity infill (45-55) stations
   -- Go/No Go Decision--
4. MT Survey (60-80 stations)
5. Development of a 3D geothermal system model
6. Siting of well(s) for future drilling by DoD

Play #5 – West Fort Bliss Play
1. Water sample collection in expanded study area for chemistry and geothermometry; logging
2. Shallow temperature survey (45-65 stations)
3. Additional gravity infill (50-70) stations

Play #6 – WSMR Uprange Play
1. Water sample collection in expanded study area for chemistry and geothermometry; logging
2. Expanded shallow temperature survey (45-65) stations)
3. Additional gravity infill (40-50) stations

Note: RMI staff has met with NEPA/Environmental Coordinators at both WSMR and ADF-SW and no significant obstacles exist related to access or clearances for our field work personnel. RMI is beginning to work with WSMR to expand/extend the existing Phase 2 REC, which would cover our proposed Phase 3 work in Plays 2, 3, 4 and 6. As before, any work performed at ADF-SW/NASA would fall under the existing REC they have developed for the new data center. Permitting for TG holes at WSMR will fall under the purview of the NM State Engineer's Office out of Las Cruces, NM. All drilling will be done on DoD land or land controlled by the Army. Field work in both areas can begin as early as Oct. 1, 2017.

Total Request From U.S. DOE for Phase 3 As Proposed: $1,497,000
Est. Match From Project Team for Phase 3 As Proposed: $375,250

TOTAL PROPOSED BUDGET FOR PHASE 3: $1,871,250*

* Estimate above includes all coordination and preparation for, as well as supervision of, on the ground testing on 2-3 separate military facilities, coordination with relevant state & federal agencies, ongoing military liaison, travel costs to test site, as well as mandatory conference and meeting expenses. The estimate also includes integration of all data into our final Phase 3 PFA models and project GIS. Project will commence on Oct 1, 2017 for approximately 16-18 months.

__Alternative to Phase 3 Estimate: Eliminating field work in plays #5 and #6 and reducing the number of slimholes at WSMR to 5 will bring the Phase 3 request from US DOE Down to approx. $965,000. Other options could include reducing the size of the MT surveys.__

References

Bonham-Carter, G., 1994. Geographic information systems for geoscientists: modelling with GIS. Pergamon press.

Broadhead, R.F., 2003, Petroleum geology of the McGregor Range Otero County, New Mexico. AAPG Search and Discovery Article #10052.

Coolbaugh, M. F., 2003: the prediction and detection of geothermal systems at regional and local scales in Nevada using a geographic information system and thermal infrared imagery. Dissertation, University of Nevada, 172 p.

Coolbaugh, M., Sladek, C., Faulds, J., Zehner, R., and Oppliger, G. "Use of Rapid Temperature Measurements at a 2-Meter Depth to Augment Deeper Temperature Gradient Drilling," Thirty-Second Workshop on Geothermal Reservoir Engineering, January 2007.

Coolbaugh, M., Sladek, C. and Kratt, C. "Compensation for Seasonal and Surface Affects of Shallow (Two-Meter) Temperature Measurements," Geothermal Resource Council Transactions, Volume 34, 2010.

Faulds, J., M. Coolbaugh, G. S. Vice, and M. L. Edwards, 2006. Characterizing structural controls of geothermal fields in the northwestern Great Basin: A Progress Report, GRC *Transactions,* v. 30, p. 69-76.

Faulds, J., M. Coolbaugh, V. Bouchot, I. Moeck, and K. Oguz, 2010. Characterizing Structural Controls of Geothermal Reservoirs in the Great Basin, USA, and Western Turkey: Developing Successful Exploration Strategies in Extended Terranes, *Proceedings*, World Geothermal Congress, Bali, Indonesia, p. 1-10.

Faulds, J. E., N. H. Hinz, C. Kreemer, and M. Coolbaugh, 2012. Regional patterns of geothermal activity in the Great Basin region, western USA: Correlation with strain rates, GRC *Transactions*, v. 36, p. 897- 901.

Faulds, J. E., N. H. Hinz, G. M. Dering, and D. L. Siler, 2013. The hybrid model – the most accommodating structural setting for geothermal power generation in the Great Basin, western USA: *GRC Transactions*, 37, 3-10.

Fournier, R. O., 1991, Water geothermometers applied to geothermal energy; in Applications of Geochemistry in Geothermal Reservoir Development, UNITAR-UNDP (ed. F. D'Amore), p. 37-69.

Fraser, A. J., 2001, Vining, B.A. & Pickering, S. C. (eds) Petroleum Geology: From Mature Basins to New Frontiers – Proceedings of the 7th Petroleum Geology Conference, 791–800. DOI: 10.1144/0070791# Petroleum Geology Conferences Ltd. Published by the Geological Society, London, p. 791-800.

Gettings, P. (2017), Ph.D. thesis, University of Utah.

Gettings, P., D. S. Chapman, and R. Allis (2008), Techniques, analysis, and noise in a Salt Lake Valley 4D gravity experiment, Geophysics, 73 (6), WA71–WA82.

Geochemistry in Geothermal Reservoir Development, UNITAR-UNDP (ed. F. D'Amore), p. 119-144.
Hinze, W. J., et al. (2005), New standards for reducing gravity data: The North American gravity database, Geophysics, 70 (4), J25–J32.

Harder, V.M., 1982, Oil and Gas Potential of the Tularosa Basin-Otero Platform Area, Otero County, New Mexico. M.S. Thesis, University of Texas at El Paso, 90 p.

King, W.E., and Harder, V.M., 1985, Oil and Gas Potential of the Tularosa Basin-Otero Platform Area, Otero County, New Mexico. New Mexico Bureau of Mines & Mineral Resources, Socorro, Circular 198, 37 p.

Kottlowski, F.E., 1975. Stratigraphy of the San Anders Mountains in south-central New Mexico. In: Las Cruces County. Seager, W.R., Clemens, R.E., Callender, J.F. (eds.), New Mexico Geological Society 26th Annual Fall Field Conference Guidebook, pp. 95-104.

Lazaro, M., Page, C., Tiedeman, A., Sabin, A., Bjornstad, B., Alm, S., Meade, D., Shoffner, J., Mitchel, K., Crowder, B. and Halsey, G."United States Department of the Navy Geothermal Exploration Leading to Shallow and Intermediate Drilling at Hawthorne Ammunition Depot, Hawthorne, NV," Geothermal Resource Council Transactions, Volume 34, 2010.

Lazaro, M., Alm, S., Tiedeman, A., Page, C., Meade, D., Shoffner, J., Bucher, K. "Department of the Navy Geothermal Exploration on Naval Air Station Fallon (NASF) Managed Lands in Dixie Valley, Nevada," Geothermal Resource Council, Volume 35, 2011.

Marshak, S. (2004) Salients, recesses, arcs, oroclines, and syntaxes – a review of ideas concerning the formation of map-view curves in fold-thrust belts. In K.R. McClay (ed.) AAPG Memoir 52, p. 131-156.

Pribnow, D., and Clauser, C. (2000) Heat and fluid flow at the Soultz hot dry rock system in the Rhine graben. Proceedings World Geothermal Congress, Kyushu-Tohoku, Japan, May 28-June 10, 2000, p. 3835-3840.

Seager, W.R. (1981) Geology of Organ Mountains and southern San Andres Mountains, New Mexico. New Mexico Bureau of Mines & Mineral Resources Memoir 26, 97 p. plus 5 maps sheets.

Sladek, C., Coolbaugh, M. and Zehner, R. "Development of 2-Meter Soil Temperature Probes and Results of Temperature Survey Conducted at Desert Peak, Nevada, USA," Geothermal Resource Council Transactions, Volume 31, 2007.

Sawatzky, D.L., Raines, G.L., Bonham-Carter, G.F., and Looney, C.G., 2009, Spatial Data Modeler (SDM): ArcMAP 9.3 geoprocessing tools for spatial data modelling using weights of evidence, logistic regression, fuzzy logic and neural networks. http://arcscripts.esri.com/details.asp?dbid=15341.

Skord, J., Sladek, C., Coolbaugh, M., Cashman, P., Lazaro, M. and Kratt, C. "2-M Probe Survey at Dixie Valley Geothermal Area," Geothermal Resource Council Transaction, Volume 35, 2011.

Sundance Engineering, 2015, Final geothermal exploration report at White Sands Missile Range New Mexico, U.S. Army Corps of Engineers Contract No. W912PP-14-P-0076, 77 p.

Webring, M. W. (1985), SAKI–a Fortran program for generalized linear inversion of gravity and magnetic profiles, Open-File Report 85-122, U.S. Geological Survey, 104p.

APPENDIX A: General Stratigraphy
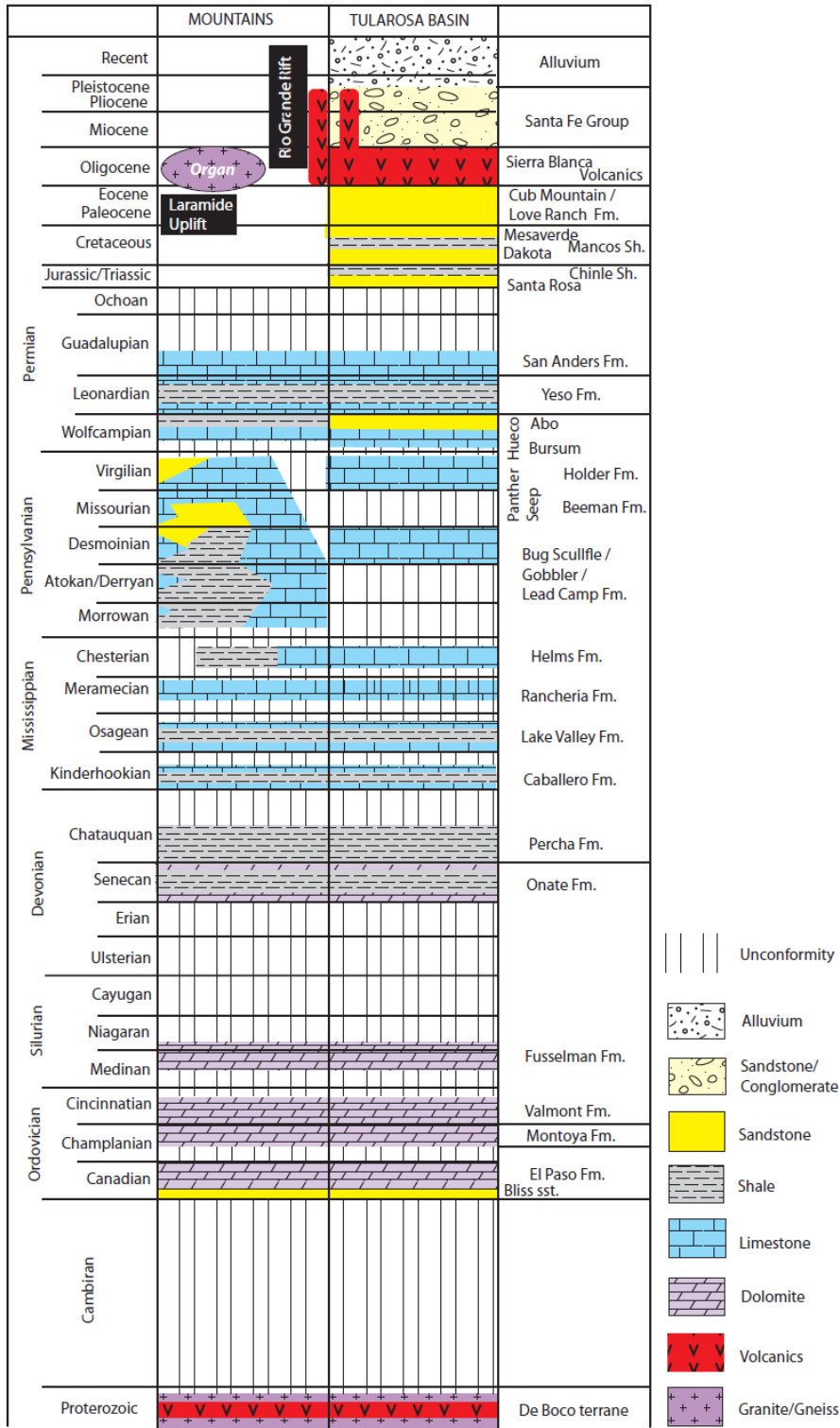
A simplified stratigraphy of the Tularosa Basin and bordering mountains in southern New Mexico (modified from Seager, 1981; Harder, 1982; King and Harder, 1985; and Broadhead, 2003).

APPENDIX B: Gravity Transect
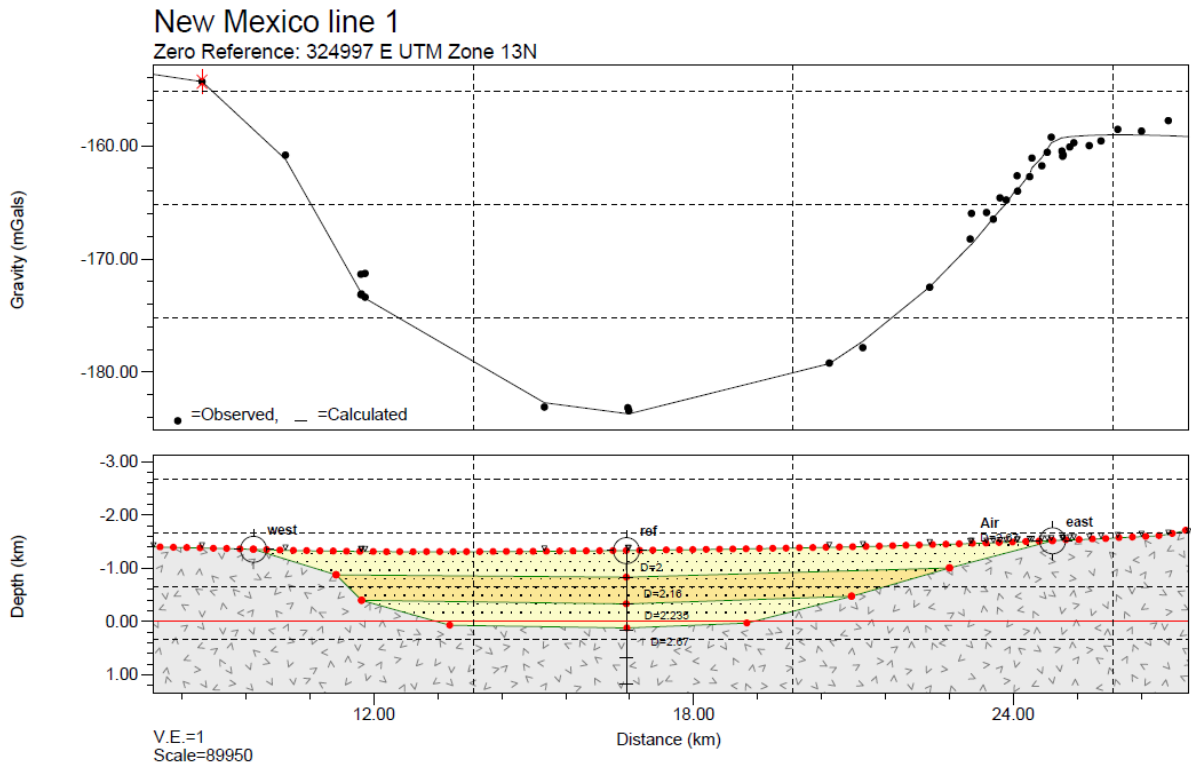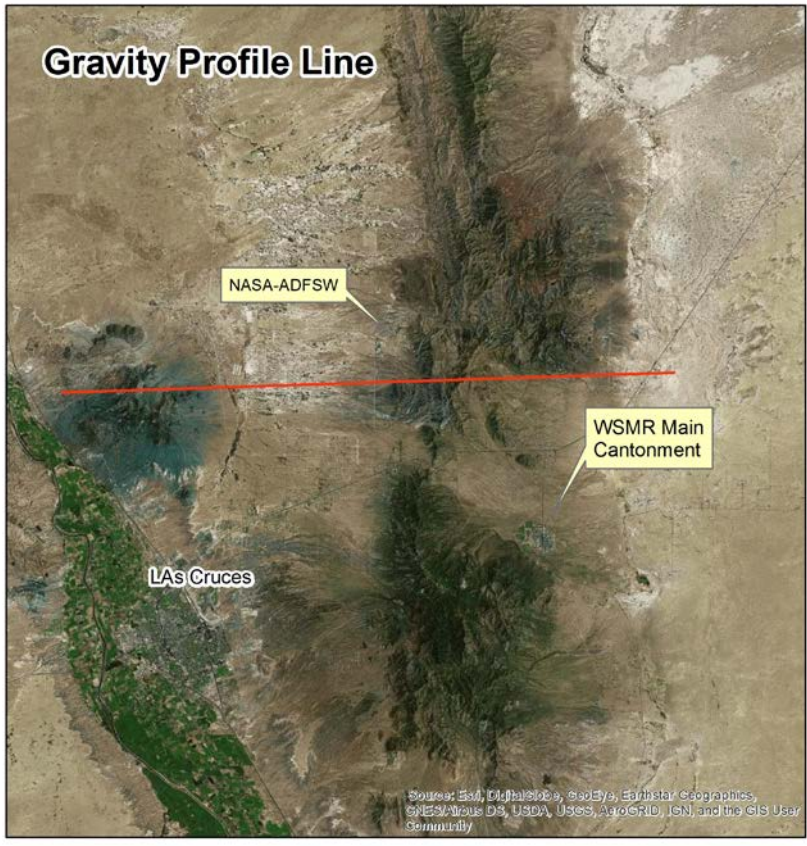
APPENDIX C: MT Inversions

Two inversions were carried out, the first using only 16 (every other) of the 31 frequencies used for the second inversion. From a starting nRMS near 12, nRMS values close to 1 were obtained by Model 11, in both inversions, from a 25 Ωm starting halfspace.

Topography

- Source: USGS (2006), Shuttle Radar Topography Mission, 1 Arc Second scene SRTM_ffB01_p032r038, Filled Finished-B 2.0, Global Land Cover Facility, University of Maryland, College Park, Maryland, February 2000.
  - ftp://ftp.glcf.umd.edu/glcf/SRTM/WRS2_Tiles/p032/SRTM_ffB01_p032r038

Mesh

- 82 (north) x 80 (east) x 61 (vertical) FE cells; 13 layers of air (z-node #14 is earth surface).
- Deformed vertically to mimic the surface topography at z-layer=14 nodes.
- 78 x 76 x 46 inversion parameters (272,688)
- Background elevation set to 1250 m asl.

Data Weights

- Kzx and Kzy are not included in the inversion.

- data weight for Z_{ij} at frequency ifr $= \max \begin{cases} 5\% \cdot \left| Z_{ij}(ifr) \right| \\ 5\% \cdot \dfrac{\left| Z_{xy}(ifr) - Z_{yx}(ifr) \right|}{2} \\ \text{originally assigned data weight} \end{cases}$

Model Weights

- Model weights are determined by the following scheme:
  - For each layer *iz*, consider parameters *j* immediately beneath and surrounding each receiver. Calculate
    - $MeanW_{iz} = \left(\dfrac{\sqrt{\sum (S_j)^2}}{\#} \right)_{iz}$; $S_j = \left(\dfrac{\sqrt{diag F^T F}}{cellvolume} \right)_j$
    - $MaxW_{iz} = \max(S_j)_{iz}$.
  - Determine shallowest layer for which $MaxW_{iz} \leq 2 \times MeanW_{iz}$; set $MaxW_{ref} = MaxW_{iz}$. Should $MaxW_{ref}$ not be defined by a user-specified *iz*, the specified *iz* is used to determine $MaxW_{ref}$.
  - For each layer, model weight applied laterally: $W_L(iz) = 1 + \dfrac{MaxW_{iz}}{MaxW_{ref}}$

model weight applied vertically: $W_V(iz) = 1 + 10\% \left(\dfrac{MaxW_{iz}}{MaxW_{ref}} \right)$.

- o Note model weights are calculated for the starting model and held fixed for the inversion.
- o Note model weights are scaled by the average volume of the cells within a user-specified region-of-interest (ROI).

Smoothness Regularization Calculation

- $\lambda = nRMS \cdot ndiagJ \cdot \kappa$

  - o $ndiagJ = \dfrac{\sum \left(J^T_{\cdot j} J_{\cdot j} \right)}{\# j}$. If *ndiagJ* increases from one iteration to the next, the smaller value is used.

  - o $nRMS = \sqrt{\dfrac{\sum \left(\dfrac{d_{obs} - d_{pre}}{d_w} \right)^2}{\# d}}$

  - o $\kappa = 0.001$; specified in the input file. If nRMS does not reduce by at least 5% from one iteration to the next, the value of κ is halved.

Parameter-step stabilizer Epsilon:

- = 0.0000001; specified in the input file; applied only to the region of interest (NOT all diagonal entries).